Aurora B phosphorylates Bub1 to promote spindle assembly checkpoint signaling

Babhrubahan Roy, Simon J. Y. Han, Adrienne N. Fontan, Ajit P. Joglekar

Summary

Accurate chromosome segregation during cell division requires amphitelic attachment of each chromosome to the spindle apparatus. This is ensured by the Spindle Assembly Checkpoint (SAC) [1], which delays anaphase onset in response to unattached chromosomes, and an error correction mechanism, which eliminates syntelic chromosome attachments [2]. The SAC is activated by the Mps1 kinase. Mps1 sequentially phosphorylates the kinetochore protein Spc105/KNL1 to license the recruitment of several signaling proteins including Bub1. These proteins produce the Mitotic Checkpoint Complex (MCC), which delays anaphase onset [3-8]. The error correction mechanism is regulated by the Aurora B kinase, which phosphorylates the microtubule-binding interface of the kinetochore. Aurora B is also known to promote SAC signaling indirectly [9-12]. Here we present evidence that Aurora B kinase activity directly promotes MCC production in budding yeast and human cells. Using the ectopic SAC activation (eSAC) system, we find that the conditional dimerization of Aurora B (or an Aurora B recruitment domain) with either Bub1 or Mad1, but not the 'MELT' motifs in Spc105/KNL1, leads to a SAC-mediated mitotic arrest [13-16]. Importantly, ectopic MCC production driven by Aurora B requires the ability of Bub1 to bind both Mad1 and Cdc20. These and other data show that Aurora B cooperates with Bub1 to promote MCC production only after Mps1 licenses Bub1 recruitment to the kinetochore. This direct involvement of Aurora B in SAC signaling is likely important for syntelically attached sister kinetochores that must delay anaphase onset in spite of reduced Mps1 activity due to their end-on microtubule attachment.

Results & Discussion

A dissection of the contributions of Bub1 and Mad1 in Mps1-driven generation of the Mitotic Checkpoint Complex (MCC)

Unattached kinetochores activate the SAC and delay anaphase onset by producing the MCC, which is a complex of four proteins: the 'closed' form of Mad2, Cdc20, BubR1/Mad3, and Bub3. MCC production is licensed by the Mps1 kinase, which according to the current understanding, sequentially phosphorylates the 'MELT' motifs in Knl1, Bub1, and Mad1 to license protein recruitment of Bub1, Mad1, and Cdc20 respectively to unattached kinetochores (Figure 1A) [3-6]. Cdc20 is also recruited by Bub1 and BubR1 through their constitutive, Mps1-independent interactions [17]. This Mps1-mediated recruitment of SAC signaling protein to the kinetochore is essential for SAC activation.

Although Mps1 plays the dominant and essential role in SAC signaling, Aurora B kinase activity is also required for maximal signaling [9-11, 18-23]. However, whether Aurora B directly phosphorylates SAC signaling proteins to catalyze MCC production has been difficult to determine. This is mainly because the Mps1 kinase and Aurora B act concurrently in unattached kinetochores, and they may phosphorylate the same signaling proteins. To circumvent these challenges, we used the ectopic SAC activation system, or eSAC. We and others have previously shown that the conditional dimerization of just the kinase domain of Mps1 with either a cytoplasmic fragment of Spc105/KNL1 containing repeating 'MELT' motifs or with Bub1 ultimately results in a kinetochore-independent activation of the SAC signaling cascade [13-16]. This eSAC signaling produces the MCC and delays anaphase onset, and therefore, provides an ideal assay for detecting the roles of Aurora B kinase activity in promoting MCC production.

Before analyzing the role of Aurora B, we used the eSAC system to clearly delineate the known roles of Mps1 in controlling the core SAC signaling cascade (summarized in Figure 1A). For this purpose, we established a simple assay to observe cell cycle progression of budding yeast cultures using flow cytometry. Flow cytometry performed on an asynchronously growing culture of haploid yeast cells reveals two peaks corresponding to 1n (G1) and 2n (G2/M) cell populations (Figure 1B). When the culture is treated with a microtubule poison such as nocodazole, the entire cell population shifts to a single peak corresponding to 2n ploidy after ~ 2 hours, indicating that the cells are arrested in mitosis (Figure S1E). After more than 2 hours of this mitotic arrest, a minor 4N peak is also evident. This peak corresponds to a population of cells that escape the mitotic block and enter the next cell cycle without undergoing cytokinesis.

We performed this assay on cells expressing Mps1-2xFkbp12 and a fragment of the Spc105 phosphodomain containing either one or six MELT motifs fused to Frb and GFP (Figure 1B). In both cases, the cell population gradually shifted to the 2n peak, which is indicative of a G2/M arrest, after introducing rapamycin into the growth media (Figure 1B, Figure S1A) [24]. Inclusion of the binding site for the Protein Phosphatase I (PP1, which antagonizes Mps1) in the phosphodomain fragment did not change the effect of rapamycin (Figure S1B). Fluorescence microscopy revealed that most cells became large-budded after two hours in rapamycin and contained two distinct clusters of bioriented sister kinetochores (Figure 1B). This morphology is consistent with cell cycle arrest in metaphase [14]. The deletion of Mad2 abrogated this arrest revealing that it was mediated by the SAC (Figure 1B, bottom left). Thus, the gradual shift of the entire cell population to 2n ploidy after rapamycin addition indicates mitotic arrest due to ectopic SAC activation.

Phosphorylation of the MELT motifs enables the recruitment of the Bub3-Bub1 complex. Therefore, we next observed cell cycle progression when Mps1 was dimerized with either Bub3 or Bub1. As expected, we observed a prolonged mitotic arrest (Figure 1C, also see Figure S1C left). The Mps1-Bub1 dimerization did not result in a cell cycle arrest when Mad2 was deleted, confirming that the arrest was mediated by ectopic SAC activation [13, 16]. Bub1 contributes two different activities to MCC formation (see schematic at the top of Figure 1C). Its central domain (residues 368-609) contains the Mad1 binding domain and a conserved ABBA motif ('486-KFNVFENF-496' in yeast) that binds Cdc20 [3, 5, 17, 25, 26]. To separate the contributions of these two activities to MCC generation, we first introduced mutations predicted to abolish Cdc20-binding to the ABBA motif (F490A,V492A,F493A,N495A, referred to as bub1^{-abba}) [25]. Induced dimerization of Mps1 with *bub1*$^{-abba}$ resulted in ectopic SAC activation suggesting that the ABBA motif in Bub1 is dispensable when ectopic SAC signaling is driven by Mps1 (Figure 1C). Cells expressing *bub1*$^{-abba}$ had a weaker but functional SAC as evidenced by their arrest in G2/M upon nocodazole treatment (Figure S1E middle and Figure 2E top right). The weakened SAC may result from the loss of Cdc20 recruitment, but it is more likely to be caused by the unexpected, ~ 50% reduction in Mad1 recruitment to unattached kinetochores (Figure S1D). This is because we saw a similar weakening of the SAC when Mad1 recruitment was similarly affected by mutations in the Mad1-recruitment domain of Bub1 (shown in Figure S2). Note that fluorescently labeled Cdc20 protein is inactive in budding yeast (data not shown). This prevented us from confirming that the ABBA motif mutations abolished Bub1-Cdc20 interaction, but results presented later support this assumption that the *bub1*$^{-abba}$ mutant is deficient in Cdc20 recruitment.

We next investigated the contribution of the phosphoregulated recruitment of Mad1 by the central domain of Bub1 (residues 368-609) to eSAC signaling [3]. In human cells, Mad1 recruitment is possible when two conserved sites, S459 and T461 of Bub1 (T453 and T455 in budding yeast Bub1), are phosphorylated by Cdk1 and Mps1 respectively [5, 6]. Previous results showed that mutation of these two residues in yeast (bub1$^{T453A,\ T455A}$) decreased Mad1 recruitment to unattached kinetochores only modestly, and did not affect the strength of SAC signaling in nocodazole-treated cells [27]. Consistently, the same mutations had no effect on the ability of Mps1 to ectopically activate the SAC in budding yeast (Fig S1E left). A prior study of the budding yeast Bub1 identified several additional phosphosites within the central domain [3]. Mutation of a subset of these sites (bub1$^{T455A,\ T485A}$ or bub1$^{T485A,\ T509A,\ T518A}$) also did not affect Mps1-driven eSAC signaling (Figure S1E middle and right). Cells expressing bub1$^{T455A,\ T485A}$ exhibited a weakened SAC when treated with nocodazole as evidenced by the emergence of a prominent 4N peak after 4 hours in media containing nocodazole (Figure S2B). Therefore, we dimerized Mps1 with a Bub1 mutant wherein all 15 phosphorylation sites (T485, T486, T487, T488, T509, T518, S537, S539, S540, T541, T555, T556, T558, T566 and S578) within the central domain were rendered non-phosphorylatable. The eSAC activity was abolished in this case (Figure 1C bottom) [3, 16]. Consistently, this Bub1 mutant did not activate the SAC upon nocodazole treatment (Figure S1F, flow cytometry right panel). It should be noted that bub1-15A itself localized to unattached kinetochores in nocodazole-treated cells (Figure S1G). These data show that the core budding yeast SAC signaling cascade relies on Mps1 phosphorylation of multiple residues within Bub1, suggesting that multiple Bub1 phosphorylation sites promote its interaction with Mad1.

We next dimerized Mps1 with Mad1 to determine whether this is sufficient to drive ectopic SAC activation. Mps1 phosphorylates Mad1 to enable Mad1-Cdc20 interaction followed by the formation of the Cdc20-closed-Mad2 dimer [5, 6]. Consistently, induced dimerization of the two proteins resulted in a prolonged mitotic arrest (Figure 1D). This eSAC activity persisted in cells expressing *spc105-6A,* wherein all six MELT motifs are non-phosphorylatable and even in cells lacking Bub3 (Figure 1D top flow cytometry panel). These results show that the ectopic SAC activation did not require the localization of Bub1 to the kinetochore and that Bub3 is not necessary for MCC formation and activity in budding yeast [28]. As suggested by the model above, Cdc20 recruitment via the ABBA motif in Bub1 was not required for eSAC activity induced by Mps1-Mad1 dimerization (Figure 1D). As expected, the dimerization of Mps1 with mad1-4A, wherein these sites are non-phosphorylatable (displayed in Figure 1D bottom flow cytometry panel), did not arrest the cell cycle, indicating that the phosphorylation sites in Mad1

implicated in the Mad1-Therefore, the Cdc20 interaction were necessary for eSAC activity. These observations suggested to us that Mps1-mediated phosphorylation of Mad1 may be sufficient to activate the SAC even in the absence of Bub1. However, Mps1-Mad1 dimerization did not elicit eSAC activity in cells expressing *bub1-15A* (Figure S1H). This observation suggests that Bub1 scaffolding for Mad1 and Cdc20 might play a role in MCC assembly (Figure S1H). This puzzling observation suggests that Bub1 plays an unknown role in promoting Cdc20-closed-Mad2 complex formation.

MCC formation also requires BubR1, known as Mad3 in in yeast. In metazoa, BubR1 is recruited to the kinetochore by Bub1 [29, 30]. However, bioinformatic analysis suggests that the Bub1-BubR1 interaction is not conserved in budding yeast [31]. To test whether BubR1 is recruited to unattached kinetochores via an unanticipated mechanism, we fused GFP to the N-terminus of Mad3 (C-terminal fusion of GFP to Mad3 makes it incompetent in SAC signaling, data not shown) and visualized its localization in nocodazole-treated cells. We did not detect significant GFP-Mad3 colocalization with unattached yeast kinetochore clusters even though it was significantly over-expressed (Figure 1E). Nonetheless, eSAC activation did not occur when Mps1 was dimerized with Mad1 in a *mad3Δ* background (Figure 1D top right). Therefore, in budding yeast, MCC formation does not require Mad3 localization to unattached kinetochores.

These observations suggest the following model for Mps1-driven SAC signaling in budding yeast. As established by previous studies, Mps1 licenses the recruitment of Bub1-Bub3 by phosphorylating MELT motifs in Spc105/KNL1, and the subsequent recruitment of Mad1-Mad2 by phosphorylating Bub1. In facilitating MCC production, Bub1-Bub3 mainly serves as a receptor for Mad1-Mad2; the recruitment of Cdc20 via Bub1 contributes to MCC formation, but it is not essential (Figure 1D, also see S1I for controls). Mps1 also phosphorylates Mad1 to license the recruitment of Cdc20, and this is essential for MCC formation. Finally, BubR1 does not localize to yeast kinetochores implying that, Cdc20-Mad2 binds BubR1 in the cytosol to form the MCC.

Testing whether Aurora B/Ipl1 kinase activity promotes MCC formation

The Aurora B kinase (known as Ipl1 in budding yeast) is implicated in SAC signaling in budding yeast. A temperature-sensitive mutant of the Aurora B kinase (*ipl1-1*) rescues the viability of *spc105*^{RASA} mutants, which otherwise cannot grow because of a severe defect in SAC silencing [32]. Ipl1 preferentially localizes to unattached kinetochore clusters in nocodazole-treated

budding yeast cells (Figure 2A, [33]). It is thus positioned to act on SAC proteins that are recruited to the kinetochore by Mps1 kinase activity. Therefore, we hypothesized that Ipl1 phosphorylates one or more of the proteins involved in SAC signaling to contribute to MCC formation.

To test our hypothesis, in strain expressing fusions of GFP-Spc105$^{120-329}$-Frb, we fused 2xFkbp12 to the C-terminus of Ipl1. To test dimerization of Ipl1 with Bub1 or Mad1, we fused FRB to the C-terminus of Ipl1 in yeast strains expressing 2xFkbp12 tagged Bub1, or Mad1. In each case, we used flow cytometry to quantify the DNA content of asynchronously growing cell cultures after the addition of rapamycin to growth media. Rapamycin-induced dimerization of Ipl1 with a Spc105 fragment spanning the six MELT motifs had no detectable effect on the cell cycle (Figure 2B top flow cytometry panel). In contrast, its dimerization with Bub1 and Mad1 resulted in a G2/M arrest (Figure 2B flow cytometry panel middle left and bottom). Examination of the spindle structure by visualizing a kinetochore-localized Spc105-GFP revealed that nearly all rapamycin-treated cells had a morphology consistent with metaphase arrest: large-budded cells with an intact spindle and two distinct, bioriented kinetochore clusters (Figure 2B microscopy image panel at the bottom). Importantly, Ipl1-Bub1 dimerization had no discernible effect on the cell cycle in *mad1Δ* mutants (Figure 2B flow cytometry panel middle right). Thus, the observed arrest required a functional SAC. These observations suggest that Ipl1 can phosphorylate Bub1, Mad1, or both to activate the SAC.

Recruitment of Cdc20 via Bub1 is essential for the Aurora B/Ipl1-mediated ectopic SAC activation

To understand the molecular mechanism of the eSAC signaling driven by Ipl1, we tested whether the known phosphorylation sites in the Mad1-binding domain of Bub1 are necessary for eSAC activation. As before, we examined cell cycle progression when Ipl1 was dimerized with non-phosphorylatable mutants of Bub1 (Figure 2C). Interestingly, when bub1^{T453A,T455A} was dimerized with Ipl1, cell cycle progression remained unperturbed indicating that eSAC activity was either significantly decreased or abolished (Figure 2C top). Dimerization of bub1^{T453A} (i.e., the Cdk1 consensus phospho-site) with Ipl1 resulted in a cell cycle arrest. Thus, the T455 residue in Bub1 is essential for Ipl1 driven eSAC signaling (Figure S2A left). Similarly, Bub1(485T) was also found to be essential to Ipl1 driven eSAC signaling (Fig. 2C, Figure S2A). In fact, the activity of these two sites is additive (Figure S2B). To test whether these

phosphorylation sites in Bub1 contribute to Mad1 recruitment to unattached kinetochores, we quantified the amount of Mad1-mCherry colocalizing with unattached kinetochore clusters in nocodazole-treated yeast cells expressing these Bub1 mutants. Mad1 recruitment was indeed reduced, but not eliminated (Figure S2D). Furthermore, the SAC was also weakened in these mutants as evidenced by their ability to grow in media containing low doses of the microtubule-destabilizing drug benomyl (Figure S2C). Together these data suggest that Ipl1 can phosphorylate sites in the Mad1-binding domain of Bub1, and that these sites contribute to kinetochore-based SAC signaling.

We next tested whether recruitment of Cdc20 via the ABBA motif in Bub1 is essential for Ipl1-driven eSAC signaling. Surprisingly, Ipl1 was unable to drive eSAC signaling when dimerized with bub1^{-abba}, as assessed by flow cytometry (Figure 2C bottom). Thus, the recruitment of Cdc20 via Bub1 is necessary for the eSAC activity induced by the dimerization of Ipl1 and Bub1. This is in contrast to Mps1, which does not require a functional ABBA motif for driving SAC signaling (Figure 1C). Thus, unlike Mps1-driven eSAC activation, the Ipl1-driven eSAC requires the Cdc20-binding activity of Bub1 for MCC assembly. These data also imply that unlike Mps1, Ipl1 may not be able to phosphorylate Mad1 to enable the Mad1-mediated Cdc20 recruitment. To test this, we dimerized Ipl1 and Mad1 in cells that either lack Bub1 (*bub1Δ*) or that express bub1^{-abba} or bub1$^{T485A,\ T509A,\ T518A}$. In each case, rapamycin treatment had no discernible effect on the cell cycle (Figure 2D). Thus, Bub1 is required for eSAC activation induced by the dimerization of Ipl1 and Mad1. These results further indicate that Ipl1 primarily phosphorylates Bub1 to facilitate ectopic MCC assembly in these experiments. Because Bub1 (T455) is predicted to be phosphorylated by Mps1, we also dimerized Ipl1 with Bub1 in a strain expressing an analog-sensitive version of the Mps1 kinase [34]. Ipl1 driven eSAC signaling was abolished when Mps1 kinase was inhibited (Figure S2E). This key observation indicates that Mps1 must prime Bub1 for Ipl1 activity. Thus, Mps1 can activate SAC in absence of Aurora B/Ipl1 activity, but Ipl1 must rely on Mps1 to promote MCC assembly [13, 14].

These data advance the following direct for Ipl1 in MCC production. Mps1 activates the SAC signaling cascade by phosphorylating the MELT motifs to license the recruitment of Bub1-Bub3. It also licenses the recruitment of Mad1-Mad2 and Cdc20 by phosphorylating Bub1 and Mad1 respectively. Ipl1 kinase also localizes within unattached kinetochores. However, it cannot activate the SAC on its own, because it cannot phosphorylate the MELT motifs. After Mps1 phosphorylates the MELT motif and primes Bub1 for Mad1 recruitment, Ipl1 can phosphorylate

Bub1 to further promote Mad1-Mad2 recruitment. Importantly, Ipl1 cannot phosphorylate Mad1 to enable the Mad1-Cdc20 interaction. It only cooperates with Bub1 to promote MCC formation.

At this juncture, it is important to note two properties of the eSAC system that likely accentuate its effect on the SAC. First, we labeled the genomic copy of Ipl1 with Frb, which means that depending on their relative abundance nearly all Ipl1 or the Fkbp12-tagged SAC signaling protein will be dimerized. Second, the high affinity dimerization of Fkbp12 and Frb domains in the presence of rapamycin will allow Ipl1 to maximally phosphorylate the signaling protein. Consequently, the eSAC system will likely reveal the maximal contribution that Ipl1 can make to SAC signaling. Under physiological conditions, this Ipl1 role is likely to be significantly smaller. Consistent with this, the SAC strength in nocodazole-treated budding yeast cells remains unchanged even when Ipl1 kinase activity is significantly reduced [35].

Evidence supporting a direct role of Aurora B/Ipl1 in driving MCC assembly in kinetochore-based SAC signaling

To detect the contribution of Ipl1 in kinetochore-based SAC signaling, we sought conditions such that Mps1 activity in the kinetochore is minimal but Bub1 is still retained within the kinetochore. As the appropriate model for this condition, we used cells expressing *spc105*^{RASA}, a well-characterized mutant of Spc105/KNL1 that cannot recruit Protein Phosphatase 1 via the 'RVSF' motif proximal to its N-terminus. In cells expressing *spc105*^{RASA}, the SAC remains active in metaphase even after kinetochore biorientation because of a greatly diminished PP1 activity [27, 32, 36]. As a result, Bub3-Bub1 is not removed from metaphase kinetochore even though the ability of Mps1 to phosphorylate Spc105 is also diminished due to the formation of stable kinetochore-microtubule attachments [14]. The concurrence of persistent Bub1 recruitment to the kinetochore with diminished Mps1 activity sets up the requisite conditions for observing the hypothesized contribution of Ipl1 to SAC signaling. Indeed, the study by Rosenberg et al. found that a hypomorphic, temperature-sensitive mutant of Ipl1 suppresses the SAC-mediated lethality of *spc105*^{RASA} cells wherein the recruitment of PP1 for SAC silencing is abrogated. This observation clearly implicates Ipl1 kinase activity in the persistent SAC signaling.

Our eSAC experiments show that the ABBA motif in Bub1 is necessary for Ipl1 mediated, but not for Mps1-mediated, SAC signaling. Therefore, we tested whether the ABBA motif in Bub1 is necessary for the persistent SAC signaling in the *spc105*^{RASA} cells. Using tetrad analysis, we found that the *bub1*$^{-abba}$ *spc105*^{RASA} double mutant is viable, indicating that the Bub1 ABBA motif

is essential for the persistent SAC signaling from bioriented kinetochores (Figure 2E, left). As expected, *bub1*$^{-abba}$ mutation did not detectably alter SAC strength in nocodazole-treated yeast cells, wherein Mps1 activity within unattached kinetochores is maximal (Figure 2E, right). We also observed similar rescue of *spc105*^{RASA} by *bub1*$^{T455A,\ T485A}$ and bub1$^{T485A,\ T509A,\ T518A}$ (Figure S2F and bub1^{T453AT455A}, see ref. [27]). These genetic interactions imply that the Bub1-mediated recruitment of both Mad1 and Cdc20 is necessary for the persistent SAC signaling from bioriented kinetochores in cells expressing *spc105*^{RASA}. Combined with the suppression of *spc105*^{RASA} lethality by *ipl1-1* (temperature sensitive mutant of Aurora B/Ipl1 in yeast), these data support our hypothesis that Ipl1 directly promotes MCC formation by phosphorylating Bub1 to promote Mad1 recruitment and relying on the ABBA motif in Bub1 for Cdc20 recruitment.

Ipl1 may phosphoregulate the Cdc20 recruited by Bub1 to promote SAC signaling. Therefore, we tested whether any of the putative phosphorylation sites in Cdc20 are necessary for SAC signaling using the rescue of *spc105*^{RASA} mutant viability as the readout. We created several phospho-null alleles of Cdc20 by mutating residues (S24, S46, S52, S62, S88, S89, S229, S602-S605) that are either known or likely to be phosphorylated (www.phosphosite.org). Tetrad analysis of diploid double mutants carrying *spc105*^{RASA} and the Cdc20 mutants showed that none of the mutations that we tested suppressed the lethality due to *spc105*^{RASA} (Figure S2G). These results suggest that the phosphorylation of Cdc20 is not essential for SAC signaling.

Aurora B drives ectopic SAC signaling in human cells

In human cells, Aurora B promotes SAC signaling through three indirect mechanisms: (1) creating unattached kinetochores, (2) potentiating Mps1 recruitment to the kinetochore [10], and (3) inhibiting phosphatase activity antagonizing Mps1 in the kinetochore [9]. Additionally, a direct involvement of Aurora B kinase activity in SAC signaling has been noted before. In human and fission yeast cells, Aurora B kinase activity is required for SAC signaling initiated by artificial tethering of Mad1 to bioriented kinetochores [37-39]. Interestingly, Bub1 is also essential for SAC activation under these conditions [40], similar to the requirement of Bub1 when Aurora B and Mad1 are dimerized in yeast cells (Figure 2D). Based on these data, we hypothesized that Aurora B can contribute SAC signaling by phosphorylating Bub1 in human cells.

To test our hypothesis, we adapted the previously described eSAC system in HeLa cells [13]. Briefly, we created HeLa cell lines that constitutively express one of the three protein fragments: KNL1 (Spc105 homolog) phosphodomain containing six MELT motifs (two tandem copies of a

fragment spanning motifs 12-14 in KNL1 also named as M3-M3; [41]), the central domain of Bub1, or the C-terminal domain of Mad1, each fused to mNeonGreen-2xFkbp12 (Figure 3A, Methods). In these cells, we conditionally expressed Frb-mCherry-INCENP$^{818\text{-}918}$ using a doxycycline-induced promotor. INCENP$^{818\text{-}918}$ binds to and is essential for the activation of Aurora B in human cells [42]. Due to the acute induction of the inducible promoter (< 48 hours prior to the start of the experiment, see Methods), the expression level of Frb-mCherry-INCENP$^{818\text{-}918}$ was lower than that of the Fkbp12-fused SAC protein fragment, and it varied from cell to cell (see Figure 3A). This variability allowed us to measure both the dose (amount of conditionally dimerized complex determined by the average mCherry fluorescence in a mitotic cell) of the Aurora B-based eSAC and the cellular response to the eSAC dosage in the form of delayed anaphase onset.

To study the effect of the induced dimerization of Frb-mCherry-INCENP$^{818\text{-}918}$ and each protein fragment, we added rapamycin to the growth media for asynchronously growing HeLa cells and imaged them for a period of ~ 24 hours (Methods). For cells that entered and completed mitosis during this period, we determined the mitotic duration as the time duration for which a HeLa cell exhibits with the rounded morphology characteristic of mitotic cells, before undergoing anaphase onset (Figure 3B). In each mitotic cell, we quantified the average mCherry signal over the entire cell and used this value as the reporter of eSAC dosage [13].

We first confirmed that the rapamycin-induced dimerization of Frb-mCherry-INCENP$^{818\text{-}918}$ with mNeonGreen-2xFkbp12 (no SAC signaling activity) did not affect the duration of cell mitosis (Figure 3D). Thus, the ectopic over-expression of INCENP$^{818\text{-}918}$ did not significantly alter mitotic duration. We found that the dimerization of INCENP$^{818\text{-}918}$ with the fragment of KNL1 containing six MELT motifs did not affect the mitotic progression (Figure 3B, left, supporting Video S1). Consistently, the MEIpT motifs (variants of the consensus ‘MELT’ sequence) in this fragment were not phosphorylated upon its dimerization with INCENP$^{818\text{-}918}$ as evidenced by the western blot analysis of the whole cell lysates probed with a phospho-specific antibody against MEIpT (Figure 3C, also see Figure S3A and S3B). The dimerization of INCENP$^{818\text{-}918}$ with either Bub1$^{231\text{-}620}$ or Mad1$^{479\text{-}725}$ resulted in a dose-dependent mitotic delay (Figure 3B, middle and right, supporting Videos S2-S3). In both cases, we quantified the maximal response as the plateau of the 4-parameter sigmoid fit to the mean values of binned data (Figure 3D, Methods). The maximal mitotic delays induced by the dimerization of Frb-mCherry- INCENP$^{818\text{-}918}$ with Bub1$^{231\text{-}620}$ and Mad1$^{479\text{-}725}$ were similar in magnitude, and also comparable to the maximal delays caused by the dimerization of the Mps1 kinase domain with the same protein fragments

(Figure 3D; data marked with an asterisk are reproduced from [13] for comparison). This is indicative of the similar activity of the eSAC systems. Thus, Aurora B can drive ectopic SAC signaling by phosphorylating either Bub1 or Mad1, or both, in HeLa cells.

We also ensured that the Aurora B driven eSAC activity is kinetochore independent. We fused Fkbp12 to Bub1$^{271-620}$ that cannot localize to kinetochores, because it lacks the 'GLEBS' motif that mediates the Bub1-Bub3 interaction and the TPR domain which can interact with Knl1/Spc105 [43, 44]. We created two cell lines expressing Bub1$^{271-620}$-2xFkbp12 and either Frb-mCherry-Mps1 kinase domain or Frb-mCherry-INCENP$^{818-918}$. In both cell lines, addition of rapamycin to the growth media resulted in a dose-dependent prolongation of mitosis (Figure 3E left). In fact, the maximal delay was slightly higher indicating that eSAC activity was stronger presumably because the Bub1 fragment does not sequester Bub3, ensuring the full availability of Bub3-BubR1 for MCC formation [45].

The ABBA motif of human Bub1 is necessary for the ectopic SAC activation by Aurora B

Our budding yeast data indicate that Mps1-driven eSAC activity does not require the ABBA motif in Bub1, but Aurora B-driven eSAC activity does. The likely explanation for this observation is that Mps1 can phosphorylate Mad1 to license Cdc20 recruitment, but Aurora B cannot do so and therefore relies on the ABBA motif for Cdc20 recruitment during SAC activation. To test whether this principle is conserved in human cells, we created two cell lines that express either Frb-mCherry-Mps1 kinase domain or Frb-mCherry-INCENP$^{818-918}$ along with Bub1$^{271-522}$, which lacks the ABBA motif. In cells expressing the Mps1 kinase domain, addition of rapamycin resulted in a clear dose-dependent delay in anaphase onset, revealing that the Mps1 kinase domain does not require the ABBA motif in Bub1 to facilitate ectopic MCC assembly (Figure 3E top right and 3F). However, the dimerization of the same fragment with Frb-mCherry-INCENP$^{818-918}$ produced a noticeably weaker response (Figure 3E bottom and 3F). These results mirror the findings from the budding yeast eSAC experiments: the ABBA motif in Bub1 is dispensable for Mps1-driven eSAC activity, but it is necessary for Aurora B-driven eSAC.

The necessity of the ABBA motif in Bub1 for Aurora B-mediated eSAC activity also implies that the mitotic delay observed upon Frb-mCherry-INCENP$^{818-918}$ dimerization with Mad1$^{479-725}$ will require Bub1-Mad1 interaction, which is dependent on Mps1 activity. The rapamycin-induced dimerization of INCENP$^{818-918}$ and Mad1$^{479-725}$ failed to delay cell division when the Mps1-

inhibitor Reversine was added to the growth media (Figure S3C). Thus, Mps1 kinase activity is critical for Aurora B-driven eSAC activity when INCENP$^{818-918}$ is dimerized with Mad1$^{479-725}$.

Aurora B kinase activity promotes MCC assembly during kinetochore-based SAC signaling

Finally, we wanted to test whether Aurora B directly promotes the core SAC signaling cascade from within unattached kinetochores independently of its indirect roles in maintaining SAC activity. To this end, we adopted the following strategy. Our eSAC data indicate that Aurora B can promote MCC formation by phosphorylating Bub1 within unattached kinetochores, but only after Mps1 licenses the recruitment of Bub1-Bub3 by phosphorylating the MELT motifs. Therefore, to detect the contribution of Aurora B to MCC formation, the following three conditions must be met: (1) Mps1 must license the recruitment of Bub3-Bub1 to unattached kinetochores and phosphorylate Bub1, (2) Mps1 activity should be reduced so that the contribution of Aurora B activity can be detected, and (3) PP1 and PP2A must be inhibited to ensure that the MELT motifs remain phosphorylated and thereby retain Bub1-Bub3 [9].

We used the following treatments to meet these three conditions. First, we released G2/S synchronized HeLa cells expressing histone H2B-RFP cells into the cell cycle, and then treated them with nocodazole to depolymerize microtubules. This treatment created cells with unattached kinetochores and active SAC. In these cells, Mps1 kinase activity was partially suppressed using 250 nM Reversine. As a result, Mps1 activity was significantly reduced, but it was still sufficient to license Bub1-Bub3 recruitment in the unattached kinetochores [41]. To satisfy the third condition: lowering PP2A activity within the kinetochore, we suppressed PP2A recruitment to the kinetochore by RNAi mediated knockdown of the five isoforms of the B56 subunit that target PP2A to the kinetochore. Additionally, we further significantly reduced phosphatase activity by combining the B56 RNAi with Calyculin A, which inhibits PP1 strongly and PP2A to a lesser extent [46].

Consistent with prior studies, the partial inhibition of Mps1 significantly reduced the duration of the average duration of the mitotic arrests induced by 330 nM nocodazole to 126 ± 100 minutes (mean ± S.D., Figure 4A, compared to > 1000 minutes in cells treated with nocodazole alone, data not shown). Disruption of PP2A recruitment to the kinetochore increased mitotic duration to 258 ± 160 minutes (mean ± S.D., Supporting Video S4) [9]. When Aurora B activity was inhibited by the addition of the small molecule inhibitor ZM447439 under the same condition, the

mitotic arrest was completely abolished, and the cells exited mitosis within 20 minutes (15 ± 6 minutes, Supporting Video S5). The addition of Calyculin A did not increase the duration of mitosis (Figure 4A). These experiments indicate that Aurora B kinase activity contributes to SAC signaling directly and independently from its indirect role in retarding SAC silencing.

In summary, our eSAC data reveal how Aurora B can directly promote MCC formation by phosphorylating Bub1 (Figure 4B). Aurora B does not activate the SAC on its own, primarily because it cannot phosphorylate the MELT motifs in Spc105/KNL1. However, after Mps1 activates the SAC by phosphorylating the MELT motifs to enable Bub1-Bub3 recruitment to the kinetochore and primes Bub1 by phosphorylating it in concert with Cdk1 [5, 6], Aurora B phosphorylates the central domain of Bub1 to promote the recruitment of Mad1-Mad2. Bub1-Mad1 binding in turn coordinates the interaction between Mad1-Mad2 and the Cdc20 molecule recruited by the ABBA motif in Bub1, which ultimately results in the formation of the closed-Mad2-Cdc20 complex, paving the way for MCC formation.

The requirement of Mps1 activity upstream from Aurora B in kinetochore-based SAC signaling and the significant overlap among the phosphorylation targets of the two kinases prevented us from testing this model more directly. Nonetheless, it explains prior observations showing that Aurora B cooperates specifically with Bub1 in promoting SAC signaling [18]. We propose that due to the inability of Aurora B to license the Mad1-Cdc20 interaction by phosphorylating Mad1, Cdc20 required for Aurora B-mediated MCC formation must be recruited via the ABBA motif in Bub1. In contrast, Mps1 phosphorylates Mad1 to license the Mad1-Cdc20 interaction to enables MCC formation [17, 18, 47]. Therefore, Bub1 and its ABBA motif are both essential for Aurora B's contribution to SAC signaling.

This role of Aurora B in directly promoting SAC signaling will be physiologically significant, specifically under conditions wherein Mps1 activity in the kinetochore is weakened. One such situation is dividing cells containing kinetochores with end-on, but syntelic, attachments (Figure 4C). End-on attachments are sufficient to suppress Mps1 activity [48-51] and weaken Mad1 recruitment via the core SAC signaling cascade and possibly through the fibrous corona [52]. Despite the lowered Mps1 activity under this condition, Aurora B, which is enriched at these kinetochores, can promote MCC formation by phosphorylating Bub1, delay anaphase onset, and thereby reduce chromosome missegregation. Consistent with this model, Aurora B and the ABBA motif in Bub1 are both essential for SAC signaling specifically in Taxol-treated cells, wherein kinetochores maintain end-on attachments [17, 18]. This direct role of Aurora B in SAC

414 signaling may also contribute to yielding a positive correlation between centromeric tension and
415 SAC signaling.

416

417

418

Acknowledgements

This work was funded by the 5R35-GM126983 from NIGMS to APJ. We thank Prof. Mara Duncan and her lab (Department of Cell and Developmental Biology, University of Michigan Medical School) for help with the plate reader assay and dissection microscope. We acknowledge all the Joglekar lab members for their constructive criticism. We specially thank our past lab member Alan A. Goldfarb who did the initial pilot assay to show that rapamycin induced dimerization of Mps1-FRB with Mad1-Fkbp12 arrests the cell cycle. The authors acknowledge that this work would not have been possible without the HeLa cell line, which was developed from Henrietta Lacks' cells taken without compensation or informed consent.

Competing interests

We declare that no competing interests exist.

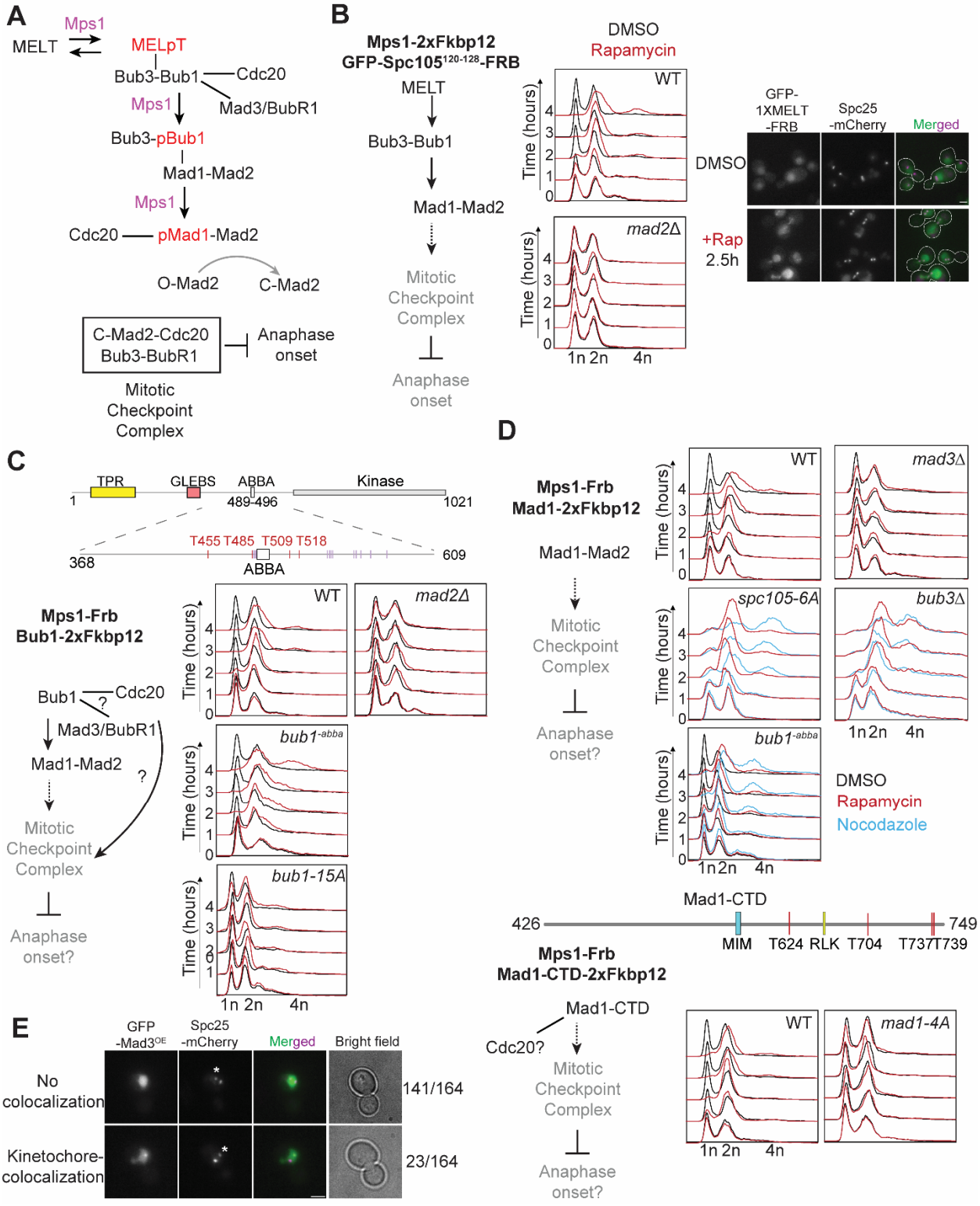

Figure 1 Dissection of the regulatory role of the Mps1 kinase in the SAC signaling cascade using the 'eSAC' system. (A) A simplified schematic of the SAC signaling cascade in budding yeast. Black arrows represent regulated recruitment of downstream signaling proteins;

black lines represent constitutive protein-protein interactions. The 'Mps1' label over an arrow signifies phosphoregulation of the protein recruitment step by Mps1. Gray arrow represents the assembly of sub-complexes into the mitotic checkpoint complex. (B) The ectopic activation of the SAC signaling cascade (simplified on the left hand) by the rapamycin-induced dimerization of Mps1-2xFkpb12 with a cytosolic fragment of Spc105 containing just one MELT motif (GFP-Spc105$^{120-128}$-Frb). Graphs on the right show the quantitation of cellular DNA content using flow cytometry over 4 hours after the addition of rapamycin to the growth media. Strain genotype is indicated at the top of each graph. Black lines show cytometry results for DMSO-treated cultures, red lines show the results for rapamycin-treated cultures. Representative micrographs of yeast cells expressing the indicated, fluorescently labeled proteins (right). Notice that the cytosolic GFP-Spc105$^{2-128}$-Frb displays faint kinetochore colocalization in rapamycin-treated cells, likely because Mps1 localizes to bioriented kinetochores [14]. Scale bar~3.2µm. (C) Top: Domain organization of Bub1 in budding yeast. Left: Schematic of the potential effects of the rapamycin-induced dimerization of Mps1-Frb with Bub1-2xFkbp12. Graphs show flow cytometry of DMSO-treated (black lines) and rapamycin-treated (red lines) cultures. (D) Top: Flow cytometry panels showing effects of rapamycin-induced dimerization of Mps1-Frb with the Mad1-2xFkbp12 in wild-type, in absence of Mad3, in presence of spc105-6A, in absence of Bub3 and in presence of bub1^{-abba}. Plot with black, red and blue lines indicate cells treated with DMSO (control), rapamycin and nocodazole respectively. Middle: Domain organization of Mad1-CTD (amino acid 426-749) in budding yeast. Bottom: In left, a partial schematic of SAC cascade is shown. In right the potential effects of the rapamycin-induced dimerization of Mps1-Frb with the Mad1-CTD-2xFkbp12 or Mad1-CTD$^{4A\ (T624A,\ T704A,\ T737A,\ T739A)}$-2xFkbp12 are shown. Color scheme as in B-C. (E) Localization of ectopically expressed GFP-Mad3 in cells arrested in mitosis due to nocodazole treatment. Note that in nocodazole-treated yeast cells typically contain two kinetochore clusters. The larger cluster is proximal to the spindle pole bodies (not visualized), and kinetochores within this cluster are attached to short microtubule stubs. The smaller cluster is distal to the spindle pole bodies (asterisk), and the kinetochores within this cluster are unattached [53]. Also see Figure S1. Scale bars ~ 3.2 µm.

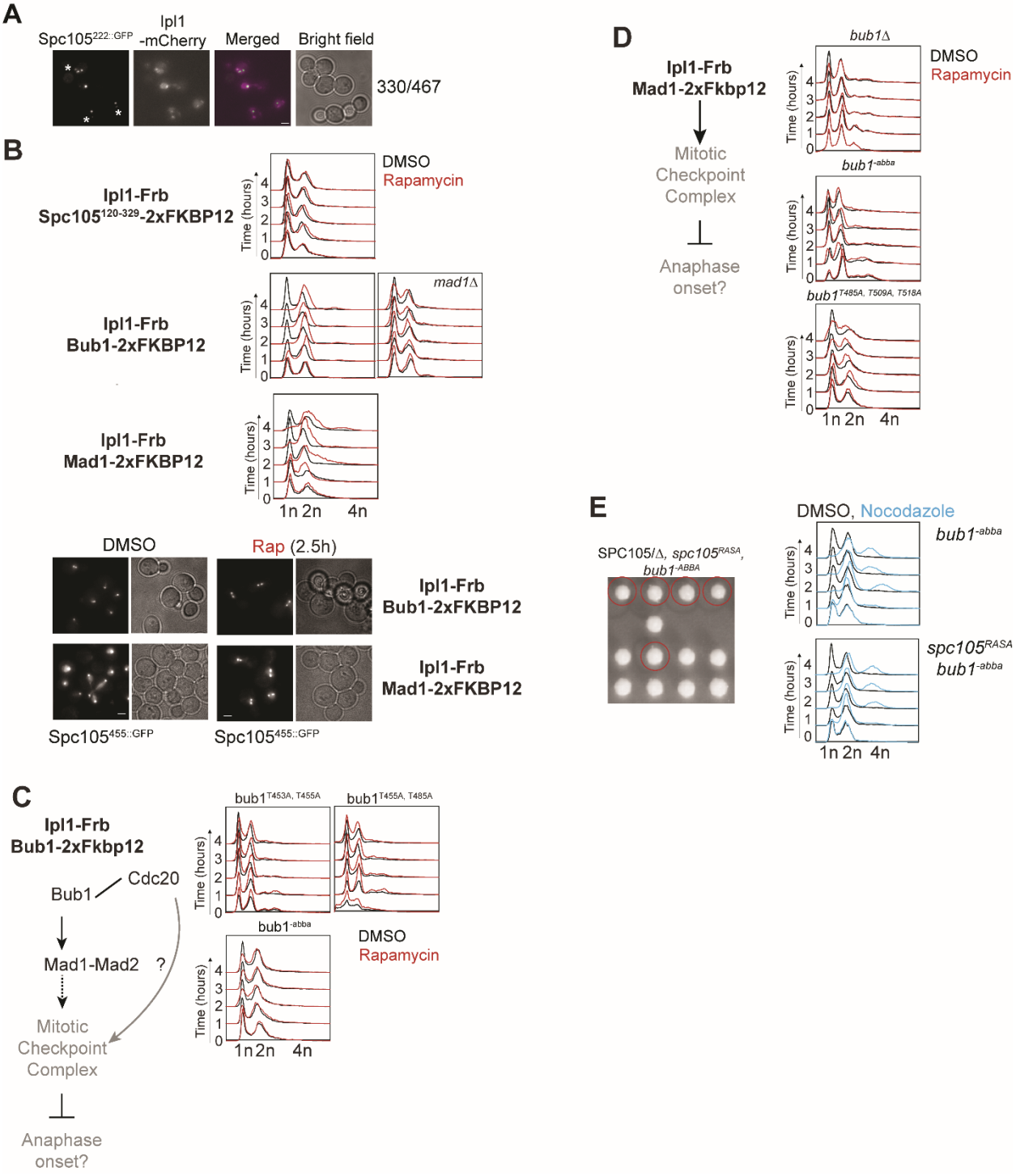

Figure 2 Rapamycin-induced dimerization of Aurora B/Ipl1 with Bub1 and Mad1, but not MELT motifs, leads to ectopic SAC activation. (A) Localization of Ipl1-mCherry and yeast kinetochores (visualized with Spc105-GFP) in yeast cells arrested in mitosis due to nocodazole treatment. Asterisks mark the cluster of unattached kinetochores in each cell. Scale bar ~ 3.2µm. (B) Left: Potential effects of the rapamycin-induced dimerization of Ipl1-Frb with the

indicated SAC signaling protein. Right: flow cytometry analysis of DMSO or Rapamycin-treated cultures of indicated strains. Color scheme as in Fig. 1. Micrographs: Morphology of rapamycin-treated cells expressing Ip1-Frb and either Bub1-2XFkbp12 or Mad1-2XFkbp12. Scale bar~3.2µm. (C) Dissection of the contributions of Bub1-mediated recruitment of Mad1 and Cdc20 in ectopic SAC signaling driven by Mps1 using Bub1 point mutants. 2xFkbp12-tagged Bub1 mutants (indicated at the top of each flow cytometry panel) expressed from the genomic Bub1 locus. (D) Flow cytometric analysis of the effect of rapamycin induced dimerization of Ipl1 and Mad1 in absence of Bub1 (*bub1Δ*, top), in presence of bub1$^{\text{-abba}}$ (middle) and in presence of bub1$^{\text{T485A, T509A, T518A}}$ (bottom) on the cell cycle. (G) Left: Tetrad dissection shows rescue of *spc105*^{RASA} by *bub1*$^{\text{-abba}}$. Right top and bottom: Flow cytometric analysis of cell cycle progression in nocodazole-treated cells carrying the indicated mutations.

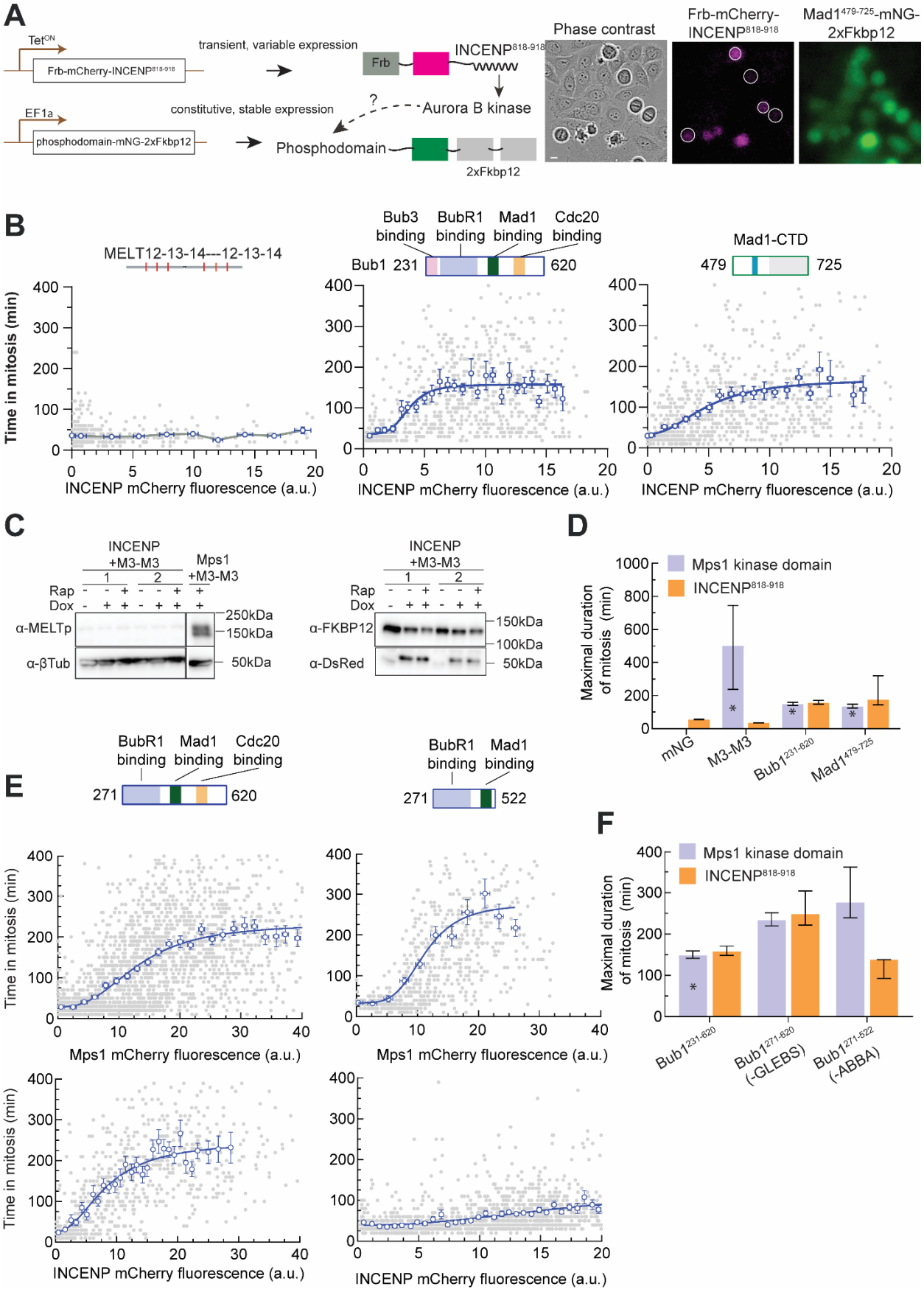

Figure 3 Rapamycin-induced dimerization of INCENP$^{818-918}$ with Bub1 and Mad1, but not with MELT motifs, leads to ectopic SAC activation in HeLa cells. (A) Left: Schematic of the eSAC system designed to test the roles of Aurora B kinase activity in the core SAC signaling cascade in HeLa cells. Right: A representative micrograph from a time-lapse experiment showing the variable expression of Frb-mCherry-INCENP$^{818-918}$. Scale bar ~ 8.25 microns. (B) Schematic at the top displays the domain organization of the eSAC phosphodomain. Scatter plots show the correlation between time in mitosis for a given cell and the average mCherry fluorescence at the beginning of mitosis for that cell. Each gray dot represents one cell (n = 520, 787, 840 respectively, data pooled from 2 experiments). The blue circles represent the mean of data binned according to the mCherry signal; the horizontal and vertical lines represent the s.e.m. For the Bub1 and Mad1-CTD fragments, the solid blue lines display a four-parameter sigmoidal fit to the binned mean values; R^2 values = 0.2, 0.2, respectively. (C) Western blot probing for the phosphorylation of the MEIT motif by Aurora B. Also see Figure S3C. (D) Bar graphs display the maximal response predicted by the 4-parameter sigmoidal fit from B. Vertical lines display the 95% confidence interval for the estimated maximal response. For comparison, the maximal response from eSAC systems comprised of the same three eSAC phosphodomains dimerized with the Mps1 kinase domain is also plotted (data marked by asterisks reproduced from [13]). Vertical lines for the M3-M3-Mps1 dimerization represent the standard deviation of the bin corresponding to the peak eSAC response. This representation was made necessary by the non-monotonic nature of the dose-response data. (E) The contributions of the Bub3- and Cdc20-binding domains in Bub1 to the observed eSAC activity driven by either the Mps1 or Aurora B (n = 2635, 614, for the top panel and n = 752, 1524 for the bottom panel; R^2 values = 0.44, 0.24, 0.51, and 0.16 respectively pooled from at least 2 experiments). The domain organization of the phosphodomain is displayed in the schematic at the top. Data presented as in B. (F) Comparison of the maximal response elicited from the indicated phosphodomains by either the Mps1 kinase domain or INCENP$^{818-918}$ (predicted mean ± 95% confidence intervals).

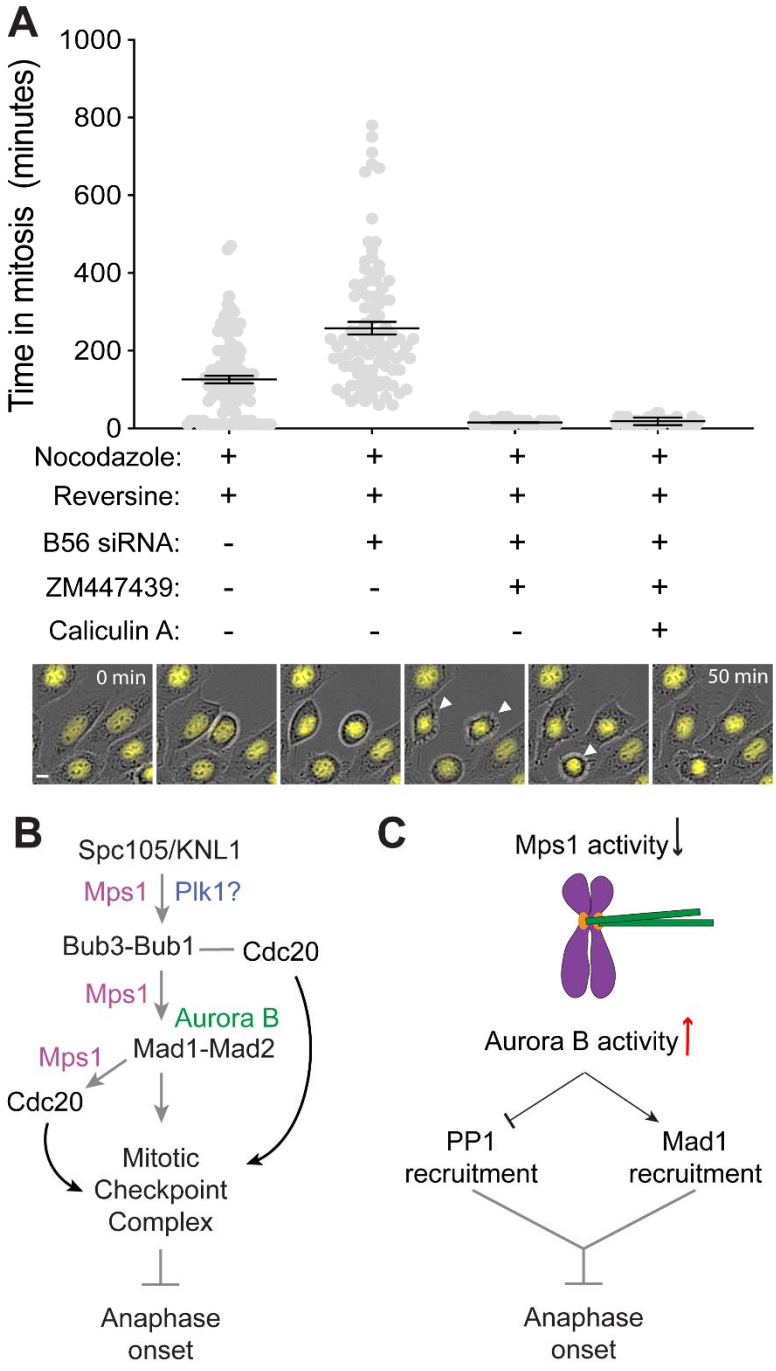

Figure 4 Aurora B contribution to kinetochore-based SAC signaling. (A) Scatter plot displays the duration of the mitotic arrest. Experimental treatments are indicted below each bar. (n = 92, 48, 43, 44, 41, experiment performed twice). Cells treated with B56 RNAi and ZM447439 both exited from mitosis very rapidly without assuming the rounded morphology. In this case, entry of the cell into mitosis was visually identified by the release of surface adhesion along with concurrent condensation of Histone H2B signal (in one experiment). Exit from mitosis

517 was identified from the re-spreading off the cell over the surface (micrograph montage at the
518 bottom, also see Supplementary Video S5). Scale bar ~ 9 microns. (B) The proposed
519 mechanism of the direct role of Aurora B kinase activity in SAC signaling. (C) Aurora B-
520 mediated promotion of MCC generation may enable kinetochores with syntelic attachments to
521 continue to produce MCC and thus delay anaphase onset.

522

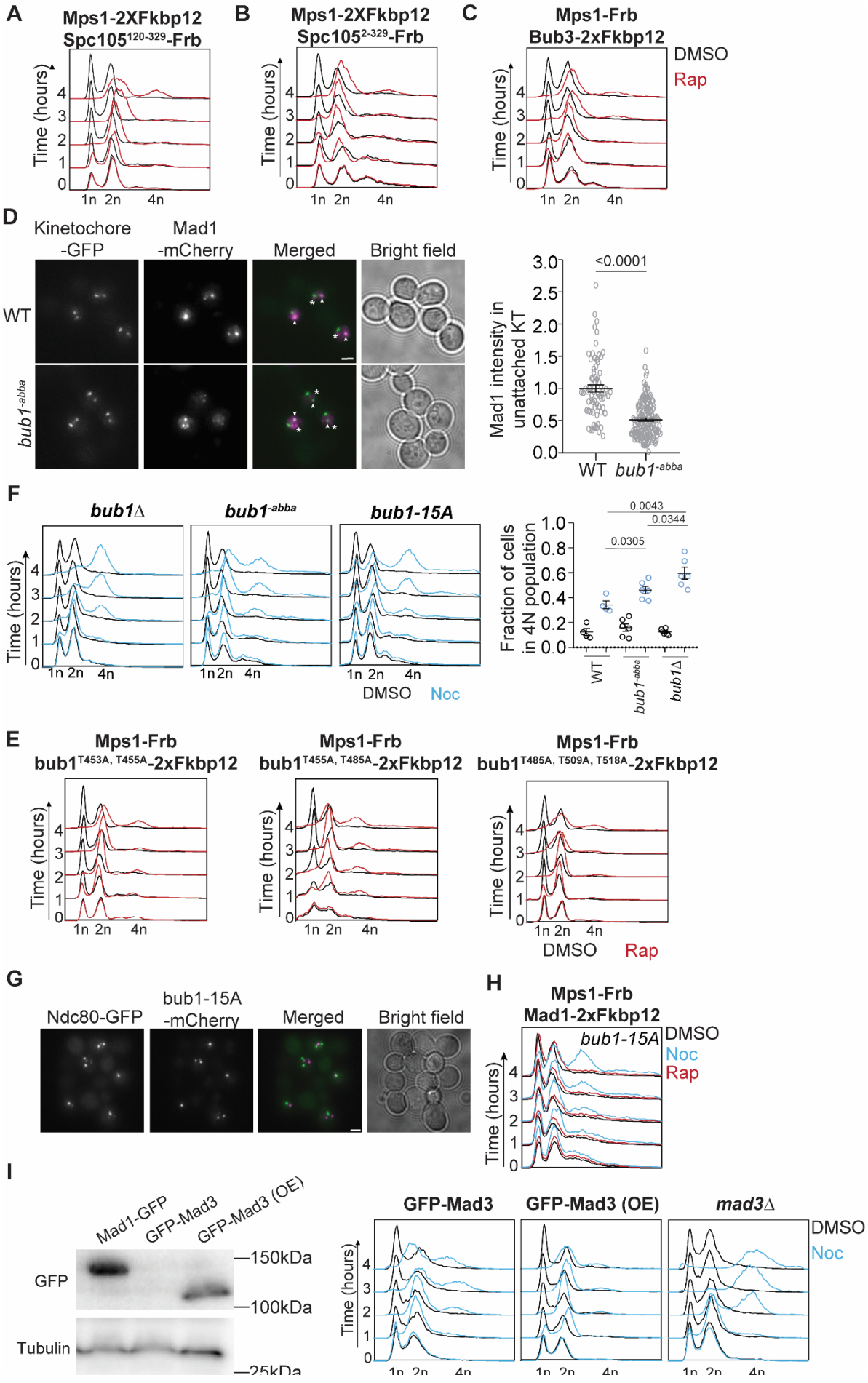

Figure S1 - **Analysis of the Mps1 kinase mediated SAC signaling cascade using the 'eSAC' system. (A-B)** Flow cytometry-based analysis of cell cycle progression following rapamycin-induced dimerization of Mps1-Fkbp12 with either GFP-Spc105$^{120-329}$-Frb, which contains six MELT repeats, or GFP-Spc105$^{2-329}$-Frb, which contains the Glc7 recruitment domain along with the six MELT repeats. **(C)** Flow cytometry analysis of cell cycle progression following the rapamycin-induced dimerization of Bub3 and Mps1 in wild-type cells. (**D**) Left: Representative images of cells with unattached kinetochore clusters showing the colocalization of the indicated proteins with fluorescently labeled kinetochores (Spc105$^{222::GFP}$ and Ndc80-GFP for WT and bub1^{-abba} respectively). Note that the Mad1-mCherry puncta marked with an asterisk result from the deletion of the nuclear pore protein Nup60. These puncta are not associated with kinetochores. The ones co-localized with kinetochores are marked with arrowheads. Scale bar ~3.2µm. Right: Scatter plot shows the quantification of fluorescence signal of kinetochore colocalized Mad1-mCherry (mean+s.e.m., normalized to the average signal measured in nocodazole-treated wild-type cells). n=72 and 151 for WT, bub1^{-abba} respectively pooled from two different technical repeats. **(E)** Flow cytometry-based assessment of cell cycle progression upon the dimerization of Mps1 with bub1$^{T453A,\ T455A}$ (left), bub1$^{T455A,\ T485A}$ (middle), or bub1$^{T485A,\ T509A,\ T518A}$ (right). **(F)** Effect of nocodazole treatment on cell cycle progression in *bub1Δ* (left), bub1^{-abba} (2nd from the left) and bub1-15A (2nd from the right) cells. Right: Scatter plot showing quantification of fraction of 4N population in WT, bub1^{-abba} and *bub1Δ* cells. The p values derived by pairwise t-tests performed on the data are mentioned on the top of the graph. **(G)** Representative microscopic images showing localization of bub1-15A-mCherry and unattached kinetochores (visualized by Ndc80-GFP) in yeast cells arrested in mitosis due to nocodazole treatment. Scale bar ~3.2µm. (**H**) Effect of nocodazole, rapamycin and DMSO (control) treatment on cell cycle progression in strain expressing Mps1-Frb, Mad1-2xFkbp12 and bub1-15A-mCherry **(I)** Left: Western analysis by α-GFP and α-Tubulin (loading control) on the lysate of Mad1-GFP, GFP-Mad3 and cells wherein GFP-Mad3 is overexpressed. Right: Flow cytometry to test the effect of nocodazole treatment on either GFP-Mad3 (left), GFP-Mad3 overexpression (middle) or *mad3Δ* cells (right).

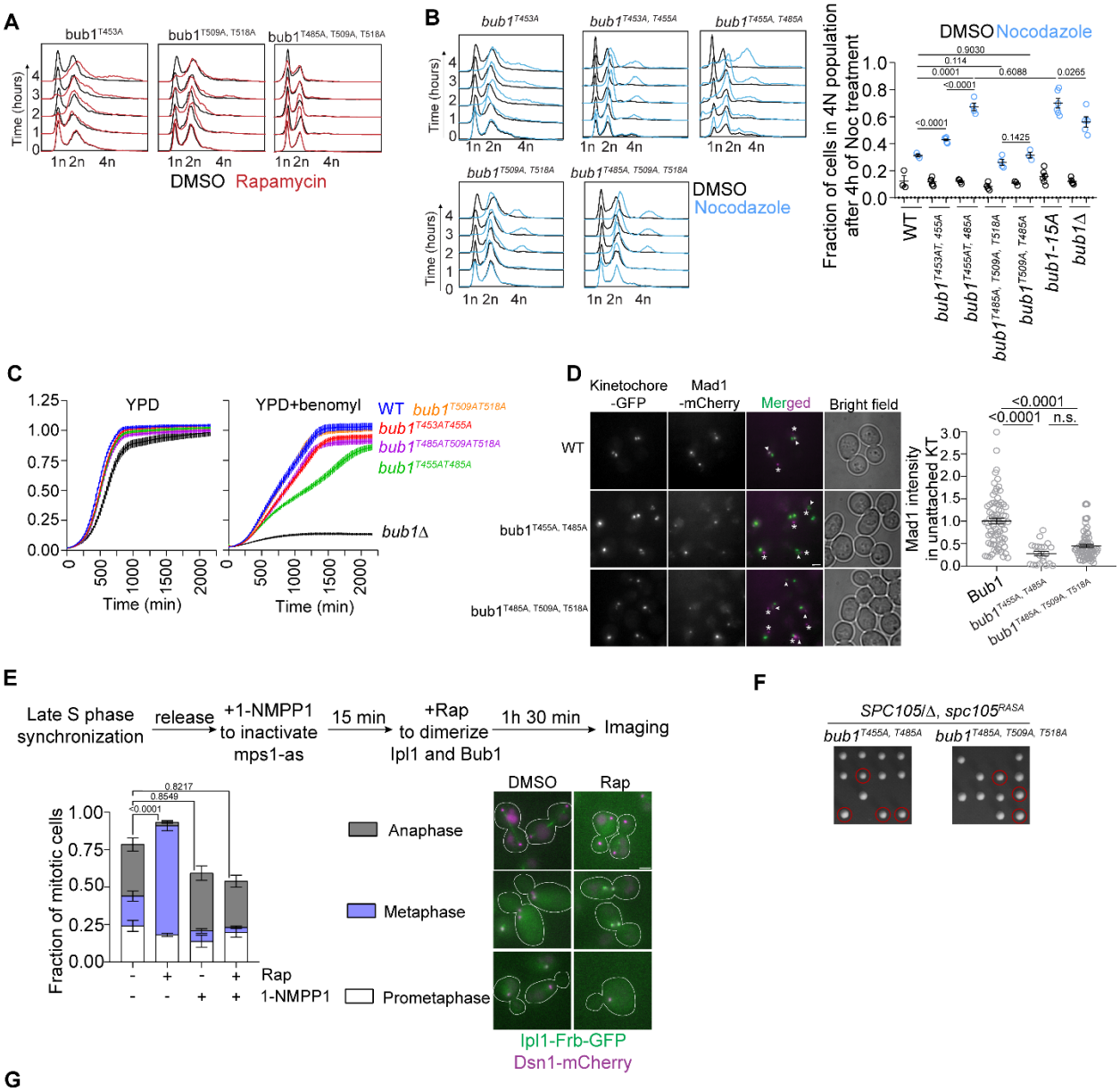

Figure S2- Dissection of the contribution of Aurora B/Ipl1 in SAC activation. (A) Effect of rapamycin induced dimerization of Ipl1 with either bub1^{T453A} (left) or bub1$^{T509A,\ T518A}$ (middle) or bub1T485A, T509A, T518A (right). **(B)** Left top and bottom: Flow cytometric profile of nocodazole treated cells of indicated strains. Cells expressing bub1$^{T455A,\ T485A}$ transition to 4n ploidy after 4 hours of exposure to nocodazole, suggesting that the mutation weakens, but does not abolish, the SAC

559 (compare with results of a similar analysis on *bub1Δ* cells in Figure S1E). Right: Scatter plot
560 depicting the fraction of cells with 4N ploidy after 4 hours of nocodazole treatment (genotypes
561 indicated below the X axis). The data were accumulated from at least three independent flow
562 cytometry experiments. The statistical significances were derived by pairwise t-tests and p
563 values are mentioned at the top. **(C)** Quantification of cell density of the indicated strains in YPD
564 media (left) and media-containing benomyl (right). bub1$^{T455A,\ T485A}$ cells (green line) stand out
565 because of their heightened sensitivity to benomyl. Note that the growth of these cells is
566 significantly better than *bub1Δ* cells (black line) under the same condition. **(D)** Left:
567 Representative images of cells with unattached kinetochore clusters showing the colocalization
568 of the indicated proteins with fluorescently labeled kinetochores (Spc105$^{222::GFP}$, Spc25-GFP and
569 Nnf1-GFP for WT, bub1$^{T455A,\ T485A}$ and bub1$^{T485A,\ T509A,\ T518A}$ respectively). Note that the Mad1-
570 mCherry puncta marked with an asterisk result from the deletion of the nuclear pore protein
571 Nup60. These puncta are not associated with kinetochores. The ones co-localized with
572 kinetochores are marked with arrowheads. Scale bar ~3.2µm. Right: Scatter plot shows the
573 quantification of fluorescence signal of kinetochore colocalized Mad1-mCherry (mean+s.e.m.,
574 normalized to the average signal measured in nocodazole-treated wild-type cells). n=74, 21 and
575 73 for WT, bub1$^{T455A,\ T485A}$ and bub1$^{T485A,\ T509A,\ T518A}$ respectively pooled from two different
576 technical repeats. n.s. Not significant. (**E**) Top: Flow chart describes the workflow to inactivate
577 Mps1 prior to dimerize Ipl1-Frb-GFP with Bub1-1xFkbp12. Bottom left: Bar graph represents the
578 fraction of mitotic when the cells expressing analogue sensitive Mps1 were treated with
579 rapamycin and 1-NMPP1 as indicated in the graph. Bottom right: representative images of
580 prometaphase, metaphase and anaphase cells as observed in untreated (DMSO) and
581 rapamycin treated cells. The number of cells analyzed in each of these 4 treatments: n=366,
582 461, 246 and 974 respectively. The whole experiment was replicated four times. The statistical
583 significances were derived by 2-way ANOVA test and p values for fractions of anaphase cells
584 are mentioned at the top of the graph. Scale bar ~3.2µm. **(F)** Tetrad dissection analysis of the
585 indicated strains. **(G)** List of mutants of putative phosphorylation sites in Cdc20, which were
586 crossed with *spc105^{RASA}*.

587

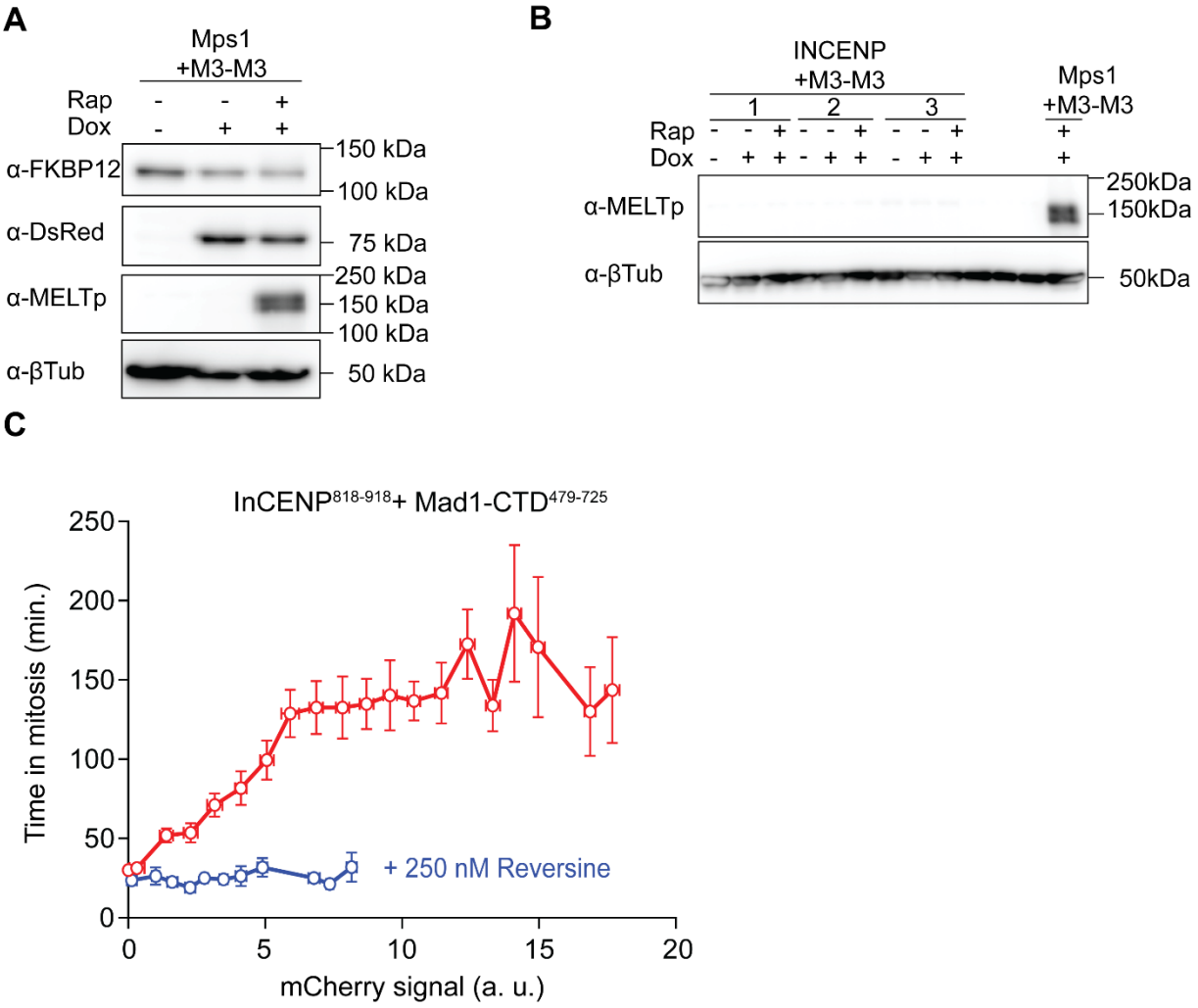

Figure S3- Rapamycin-induced dimerization of INCENP$^{818-918}$ with bub1$^{231-620}$ requires Mps1 function to mediate SAC activation. (A) Control western blot analysis for the phosphorylation of the MEIT motif by Mps1**.** The assay was repeated twice. Molecular weight markers are mentioned on the right. **(B)** Immunoblot assay to analyze phosphorylation of MEIT motif by Aurora B (Frb-mCherry-INCENP$^{818-918}$). Three biological replicates were run in this gel. Here we treated the cells as indicated in the figure. As a control, we ran the lysate of doxycycline and rapamycin treated cells that express Frb-mCherry-Mps1 kinase and M3-M3-mNeongreen-2xFkbp12. Top blot was probed with α-MEITp antibodies and bottom one was probed with α-βTubulin antibodies. The molecular weight markers are mentioned on the right. **(C)** Partial inhibition of Mps1 due to Reversine treatment (250 nM, blue line) abolishes eSAC activity induced by the dimerization of INCENP$^{818-918}$ with Mad1$^{479-725}$(n = 154, experiment performed once). Red points and line show DMSO treated cells (data re-plotted from Figure 3B).

Supplementary Videos Legend

Video S1 – Effect of rapamycin induced dimerization of Frb-mCherry-INCENP$^{818-918}$ and M3-M3-mNeonGreen-2xFkbp12 on the duration of mitosis in HeLa A12 cells (hh:mm). Images acquired on the ImageExpress Nano microscope.

Video S2 – Effect of rapamycin induced dimerization of Frb-mCherry-INCENP$^{818-918}$ and M3-Bub1$^{231-620}$-mNeonGreen-2xFkbp12 on the duration of mitosis in HeLa A12 cells (hh:mm). Images acquired on the Incucyte microscope.

Video S3 – Effect of rapamycin induced dimerization of Frb-mCherry-INCENP$^{818-918}$ and M3-Mad1$^{479-725}$-mNeonGreen-2xFkbp12 on the duration of mitosis in HeLa A12 cells (hh:mm). Images acquired on the Incucyte microscope.

Video S4 – Cell cycle progression of H2B-RFP expressing HeLa A12 cells treated with 330 nM nocodazole, 250 nM Reversine, and a cocktail of siRNA against five B56 isoforms (hh:mm). Images acquired on the Incucyte microscope.

Video S5 – Cell cycle progression of H2B-RFP expressing HeLa A12 cells treated as in S4 and 10 μM ZM447439 (hh:mm). Images acquired on the Incucyte microscope.

Materials and methods

Plasmid and strain construction

The plasmids and *S. cerevisiae* strains and cell lines used in this study are tabulated in supplementary table S1, S2 and S3 respectively. *S. cerevisiae* strains containing multiple genetic modifications were constructed using standard yeast genetics. Proteins tagged with GFP(S65T) and mCherry or yeast codon optimized mCherry were used to visualize kinetochores, spindle pole bodies and SAC signaling components. A 7-amino-acid peptide (sequence: 'RIPGLIN') was used as the linker between the proteins and their C-terminal tags (GFP, mCherry, Frb or 2xFkbp12). The cassettes for gene deletion, gene replacement and C-terminal tags were introduced at the endogenous locus through homologous recombination of PCR amplicons or using linearized plasmids [54]. In the past, we observed a significant strain to strain variation in the intensity of mCherry-tagged kinetochore proteins or checkpoint proteins due to inherent variability of the mCherry brightness. Therefore, we created all Mad1-mCherry strains by crossing the same transformant of Mad1-mCherry (AJY1836 or AJY3741) with other strains. The deletion mutant of *NUP60* always accompanies Mad1-mCherry to disrupt Mad1localization to the nuclear envelopes [55]. This facilitated clearer imaging and quantification of Mad1 localized to the unattached kinetochores without affecting SAC strength.

To create any diploid yeast strains, we mixed overnight grown cultures of two strains of a and α mating types and spotted the cell suspension on a YPD plate, and then incubated the cells for approximately 3-4 hours at 32°C. To induce meiosis or sporulation of the diploid yeast, we transferred stationary phase diploid cells to starvation media (yeast extract 0.1%, Potassium acetate 1%), and we incubated them at RT for 4-5 days.

All the Spc105 mutants that were used in the study, are chimeras of Spc105 and either GFP or codon optimized mCherry as described previously [27, 36]. Genes encoding the chimeric proteins were introduced using a cassette that consists of the 397 bp upstream and 250 bp downstream sequences of the SPC105 open reading frame as promoter (*prSPC105*) and terminator (*trSPC105*) sequences respectively. We introduced genes encoding GFP (S65T) at the 222nd amino acid position of Spc105 by sub-cloning where we introduced an extra *Bam*HI site (Gly-Ser) at the upstream and *Nhe*I site (Ala-Ser) at the downstream of the GFP fragment. The plasmids based on pRS305 or pRS306 backbone were linearized by *Bst*EII or *Stu*I before transformations to ensure their integration at the *LEU2* or the *URA3* locus respectively.

To build *bub1* phosphomutants containing plasmids, we used the pSK954 plasmid backbone [56]. pSK954 harbors the *ADH1* transcription terminator cloned within *Asc*I-*Bgl*II sites. We cloned the 500bp upstream sequence that harbors *BUB1* promoter, 3.063kb *BUB1* ORF sequence harboring the designated mutations and 651bp *2xFKBP12* or 705bp yeast mCherry within *Sac*II-*Asc*I site of this plasmid. The ORF and *2xFKBP12* or mCherry are linked by 21bp linker which codes for RIPGILK. We also cloned 350bp downstream sequence of *BUB1* which consists of *BUB1* terminator within *Pme*I-*Apa*I. To build the strains with *bub1* phosphomutant allele, we first created a diploid strain where one copy of *BUB1* was deleted with *NAT1* (AJY6055). The plasmids were digested by *Apa*I and *Sac*I to release 6.279kb fragment which recombined at the deleted bub1 locus replacing the *NAT1* cassette. There are two chimeras that express bub1$^{T453A,\ T455A}$ (pAJ852 and pAJ896). *BUB1* ORF of pAJ852 harbors mutations of 449SR450::TG. However, upon testing there were no discernable phenotypic differences between the strains constructed by pAJ852 and pAJ896.

Similarly, to construct the mutants of putative phosphorylation sites of Cdc20, we cloned the 506bp upstream sequence containing *CDC20* promoter, 1.833kb *CDC20* ORF sequence harboring the designated mutations within *Sac*II-*Asc*I sites of pSK954. We inserted *Spe*I site (ACTAGT) between the promoter and the ORF sequence. We also cloned 300bp downstream sequence of *CDC20* harboring of *CDC20* terminator within *Pme*I-*KpnI* sites. To build the strains with *cdc20* phosphomutant allele, we first created a diploid strain where one copy of *CDC20* was deleted with *TRP1* (AJY5249). The plasmids were digested by *Kpn*I and *Sac*II to release 4.328kb fragment which recombined at the deleted *cdc20* locus replacing the *TRP1* cassette.

Yeast Cell culture

Yeast strains were grown in YPD (yeast extract 1%, peptone 2%, dextrose 2%) or synthetic media supplemented with 2% dextrose (as per requirement of the yeast strain) at 32°C.

For the experiment involving analog sensitive Mps1, we grew yeast cultures for 3h till they attend mid-log phase. These cultures were treated with Hydroxyurea (100mM final) for 2h 30min to synchronize the cells late S phase. Following that, the cells were washed with YPD and released into either YPD (control) or YPD supplemented with 1-NMPP1 (50µM final). After 15min of incubation with 1-NMPP1, either DMSO (control) or rapamycin (1 µg/ml; to mediate the dimerization of Aurora B/Ipl1-Frb-GFP and Bub1-2xFkbp12) was added to the media. We categorized the mitotic cells as the prometaphase, metaphase and anaphase cells according to

681 the distribution of fluorescently labeled kinetochores within each cell (representative images in
682 Fig. S2E). The unbudded cells were considered as the cells in G1 and thus they were not taken
683 into consideration in our analysis.

684

685 **Benomyl sensitivity and 96 well plate liquid culture assay**

686 The experiment was performed as described previously [27]. Briefly, we started cultures at 0.05
687 OD_{600} in each well by appropriately diluting mid-log phase cultures maintaining ~ 160 µl final
688 volume. For assay involving benomyl treatment, cells from mid-log phase cultures were
689 pelleted, resuspended and diluted in YPD+benomyl liquid (30µg/ml). For each strain, we set at
690 least three 3 technical repeats in YPD or YPD+benomyl. We placed the 96 well plate in a
691 Spectra Max 340PC plate reader and incubated it for either 24h (YPD) or 36h (YPD+benomyl)
692 at 30°C without shaking to measure OD_{600} continuously. The reader measured the absorbance
693 every 20mins.

694

695 **Flow cytometry**

696 To perform these experiments, we started from overnight inoculum the designated strains to
697 obtain mid log phase cultures. We supplemented the media with Nocodazole (final
698 concentration 15µg/ml) to depolymerize the spindle microtubules and activate the SAC and
699 rapamycin (1 µg/ml) to induce the dimerization of FRB and Fkbp12 fused proteins [57]. We
700 collected samples containing approximately 0.1 OD_{600} cells at 0, 1, 2, 3 and 4h after addition of
701 the drug, fixed the cells using 75% ethanol, and stored them in 4°C overnight. Next day, we
702 washed out the ethanol, and treated the cells with bovine pancreatic RNase (Millipore Sigma,
703 final concentration 170ng/µl) at 37°C for 24h in RNase buffer (10mM Tris pH8.0, 15mM NaCl).
704 Then we removed the RNase and resuspended the samples in 1X phosphate buffered saline
705 (pH 7.4) and stored them in 4°C. We incubated these samples in Propidium Iodide (Millipore
706 Sigma, final concentration 5µg/ml in PBS) for at least 1h at RT on the day of the assay. The
707 stained cells were analyzed using the LSR Fortessa (BD Biosciences) in Biomedical research
708 core facility, University of Michigan medical school. We repeated flow cytometry for each strain
709 at least twice. Representative results from one of these experiments are displayed in each
710 panel. The data was analyzed using the FlowJO software and the graphs were adjusted by

Adobe illustrator. As a control for SAC null strains, we utilized *bub1Δ* or *mad2Δ* strains which revealed high number of 4N population after 4h of incubation with the nocodazole in media.

Microscopy and image analysis

We used A Nikon Ti-E inverted microscope with a 1.4 NA, 100X, oil-immersion objective for all imaging experiments. We also used the 1.5X opto-var lens to measure Mad1-mCherry intensities. The cells were imaged at room temperature in synthetic dextrose (or synthetic galactose media whenever it was required for the assay) supplemented with essential amino acids to obtain at least 20 microscopic fields at a given time points for any strains. We supplemented the mounting media with nocodazole to image the nocodazole arrested cells. For each field of view, a ten-plane Z-stack was acquired (200nm separation between adjacent planes), and at least 20 fields were acquired in each experiment.

Total fluorescence intensities of kinetochore clusters (16 kinetochores in metaphase) was measured by integrating the intensities over a 6x6 region centered on the maximum intensity pixel. We utilized the median intensity of pixels immediately surrounding or a nearby 6x6 area to correct for background fluorescence. Fluorescence intensity was calculated as described previously [58, 59].

Tissue culture and generation of stable cell lines

Henrietta Lacks (HeLa) cells were grown in DMEM media with 10% FBS, 1% Pen/Strep, and 25 mM HEPES at 37 °C and 5% CO2. Stable cell lines expressing the two eSAC components were generated by integrating a bi-cistronic eSAC plasmid at an engineered loxp site in the HeLa genome according to the protocol described in [60]. Clones with stable integration of the eSAC plasmid were selected using Puromycin (1 ug/ml), and several clones were pooled together to create the cell cultures used in the experiments.

The plasmids used for the stable cell lines were based on the plasmids that have been described previously [13]. Briefly, the phosphodomain was integrated into the constitutively expressed ORF of the plasmid using either *Not*I or *Asc*I and *Xho*I restriction sites. The INCENP$^{818\text{-}918}$ fragment was integrated into the conditionally expressed ORF using *Fse*I and *Bgl*II restriction sites.

To conduct dose-response analysis, each eSAC cell line was plated ~ 40-48 hours prior to the start of the experiment in DMEM media without Puromycin. Doxycycline was added at the time of plating to induce the expression of either Frb-mCherry-Mps1 or Frb-mCherry-INCENP$^{818-918}$. Prior to imaging, the cells were washed with PBS. Fluorobrite media with 10% FBS, 1% Pen/Strep with or without Rapamycin were added to each well.

Drug treatments and RNAi for experiments with human cells

To induce the expression of either mCherry-Frb-Mps1 kinase domain or -INCENP818-918, doxycycline was added to a final concentration of 2 ug/ml (stock concentration 2 mg/ml in DMSO). To induce the dimerization of protein fragments, Rapamycin was added ~ 1 hour prior to the start of the experiment to a final concentration of 500 nM (stock concentration 500 µM in DMSO). Partial Mps1 inhibition was achieved by adding Reversine to the final concentration of 250 nM (stock concentration 500 µM in DMSO). Nocodazole was added to the final concentration of 330 nM (stock concentration 330 µM in DMSO). ZM447439 was added to the final concentration of 10 µM (stock concentration 3mM in DMSO). Calyculin A was added to the final concentration of 100nM (stock concentration 50µM in DMSO). The cocktail of siRNA against five different B56 isoforms was added to a final concentration of 40 nM (stock concentration 10 µM). The siRNA sequences were obtained from ref. [9].

Long term live Cell Imaging of HeLa cells and Image analysis

Imaging was conducted over a period of 24 hours as described in detail previously [13]. We used either the Incucyte Zoom Live Cell Imaging system (Sartorus Inc.) or the ImageExpress Nano live cell imaging system (Molecular Devices) using 20x Phase objectives. To image cells on the Incucyte system, cells were plated in 12-well plastic tissue culture plates, whereas they were plated in 24-well plate glass-bottom dishes for imaging using the ImageExpress Nano system. Typically, 4 positions were selected within each well for imaging. At each position, one phase, GFP, and mCherry image was acquired every 10 minutes. The exposure time for mCherry image was adjusted to minimize photobleaching while ensuring accurate determination of cellular intensity values. It should be noted that the excitation intensity of the Incucyte instrument declined significantly over the course of this study. Furthermore, a small minority of the experiments were carried out on the ImageExpress Nano microscope, which has excitation

sources, optics, and detector that are entirely different from the components of the Incucyte microscope. Therefore, the mCherry intensity values across different experiments are not directly comparable. The duration of mitosis and GFP and mCherry fluorescence per cell were determined using a custom image analysis script implemented by a Matlab graphical user interface as described previously [13].

Immunoblotting

Western blotting was performed using commercial antibodies; α-GFP, JL-8 [Living Colors], 1: 3,000; α-Ds-Red [SantaCruz Biotechnologies], 1: 2,000; α-βTubulin [Sigma Aldrich, T7816], 1: 15,000; α-Fkbp12 [Abcam, ab2918], 1: 5,000; α-PhosphoMELT (MElpT, MELT13/17) [GenScript], 1: 2000. The primary antibodies were detected using HRP conjugated secondary antibodies (1: 10,000) per the manufacturer's instructions. The subsequent chemiluminescence was detected using the C600 imager from Azure Biosystems.

Statistical analysis

The technical replicates represent the number of times each experiment was performed. The biological replicates are defined as multiple transformants or segregants of the same strain which contain identical genotype. For imaging experiments, the number of cells analyzed for each strain and number of experimental replications is noted in the figure legends. All statistical analysis was performed using Graphpad Prism (version 8). We normalized the data with the mean intensities obtained for wild-type controls in each experiment to prepare the scatter plots of Mad1 intensities. To compare sample means in all other cases, we applied either the t-test or two-way ANOVA test to ascertain the statistical significance of the rest of the data using Graphpad Prism (version 8). The p-values obtained from these tests are indicated in the figures.

References

1. Musacchio, A. (2015). The Molecular Biology of Spindle Assembly Checkpoint Signaling Dynamics. Curr Biol *25*, R1002-1018.
2. Lampson, M.A., and Cheeseman, I.M. (2011). Sensing centromere tension: Aurora B and the regulation of kinetochore function. Trends Cell Biol *21*, 133-140.
3. London, N., and Biggins, S. (2014). Mad1 kinetochore recruitment by Mps1-mediated phosphorylation of Bub1 signals the spindle checkpoint. Genes Dev *28*, 140-152.
4. London, N., Ceto, S., Ranish, J.A., and Biggins, S. (2012). Phosphoregulation of Spc105 by Mps1 and PP1 regulates Bub1 localization to kinetochores. Curr Biol *22*, 900-906.
5. Ji, Z., Gao, H., Jia, L., Li, B., and Yu, H. (2017). A sequential multi-target Mps1 phosphorylation cascade promotes spindle checkpoint signaling. Elife *6*.
6. Faesen, A.C., Thanasoula, M., Maffini, S., Breit, C., Muller, F., van Gerwen, S., Bange, T., and Musacchio, A. (2017). Basis of catalytic assembly of the mitotic checkpoint complex. Nature.
7. Tipton, A.R., Ji, W., Sturt-Gillespie, B., Bekier, M.E., 2nd, Wang, K., Taylor, W.R., and Liu, S.T. (2013). Monopolar spindle 1 (MPS1) kinase promotes production of closed MAD2 (C-MAD2) conformer and assembly of the mitotic checkpoint complex. J Biol Chem *288*, 35149-35158.
8. Hewitt, L., Tighe, A., Santaguida, S., White, A.M., Jones, C.D., Musacchio, A., Green, S., and Taylor, S.S. (2010). Sustained Mps1 activity is required in mitosis to recruit O-Mad2 to the Mad1-C-Mad2 core complex. J Cell Biol *190*, 25-34.
9. Nijenhuis, W., Vallardi, G., Teixeira, A., Kops, G.J., and Saurin, A.T. (2014). Negative feedback at kinetochores underlies a responsive spindle checkpoint signal. Nat Cell Biol *16*, 1257-1264.
10. Saurin, A.T., van der Waal, M.S., Medema, R.H., Lens, S.M., and Kops, G.J. (2011). Aurora B potentiates Mps1 activation to ensure rapid checkpoint establishment at the onset of mitosis. Nat Commun *2*, 316.
11. Pinsky, B.A., Kung, C., Shokat, K.M., and Biggins, S. (2006). The Ipl1-Aurora protein kinase activates the spindle checkpoint by creating unattached kinetochores. Nat Cell Biol *8*, 78-83.
12. Nijenhuis, W., von Castelmur, E., Littler, D., De Marco, V., Tromer, E., Vleugel, M., van Osch, M.H., Snel, B., Perrakis, A., and Kops, G.J. (2013). A TPR domain-containing N-terminal module of MPS1 is required for its kinetochore localization by Aurora B. J Cell Biol *201*, 217-231.
13. Chen, C., Whitney, I.P., Banerjee, A., Sacristan, C., Sekhri, P., Kern, D.M., Fontan, A., Kops, G., Tyson, J.J., Cheeseman, I.M., et al. (2019). Ectopic Activation of the Spindle Assembly Checkpoint Signaling Cascade Reveals Its Biochemical Design. Curr Biol *29*, 104-119 e110.
14. Aravamudhan, P., Goldfarb, A.A., and Joglekar, A.P. (2015). The kinetochore encodes a mechanical switch to disrupt spindle assembly checkpoint signalling. Nat Cell Biol *17*, 868-879.
15. Yuan, I., Leontiou, I., Amin, P., May, K.M., Soper Ni Chafraidh, S., Zlamalova, E., and Hardwick, K.G. (2017). Generation of a Spindle Checkpoint Arrest from Synthetic Signaling Assemblies. Curr Biol *27*, 137-143.
16. Leontiou, I., London, N., May, K.M., Ma, Y., Grzesiak, L., Medina-Pritchard, B., Amin, P., Jeyaprakash, A.A., Biggins, S., and Hardwick, K.G. (2019). The Bub1-TPR Domain Interacts Directly with Mad3 to Generate Robust Spindle Checkpoint Arrest. Curr Biol *29*, 2407-2414 e2407.
17. Di Fiore, B., Davey, Norman E., Hagting, A., Izawa, D., Mansfeld, J., Gibson, Toby J., and Pines, J. (2015). The ABBA Motif Binds APC/C Activators and Is Shared by APC/C Substrates and Regulators. Developmental Cell *32*, 358-372.
18. Morrow, C.J., Tighe, A., Johnson, V.L., Scott, M.I., Ditchfield, C., and Taylor, S.S. (2005). Bub1 and aurora B cooperate to maintain BubR1-mediated inhibition of APC/CCdc20. J Cell Sci *118*, 3639-3652.

19. Ditchfield, C., Johnson, V.L., Tighe, A., Ellston, R., Haworth, C., Johnson, T., Mortlock, A., Keen, N., and Taylor, S.S. (2003). Aurora B couples chromosome alignment with anaphase by targeting BubR1, Mad2, and Cenp-E to kinetochores. J Cell Biol *161*, 267-280.
20. Santaguida, S., Vernieri, C., Villa, F., Ciliberto, A., and Musacchio, A. (2011). Evidence that Aurora B is implicated in spindle checkpoint signalling independently of error correction. EMBO J *30*, 1508-1519.
21. Vanoosthuyse, V., and Hardwick, K.G. (2009). A novel protein phosphatase 1-dependent spindle checkpoint silencing mechanism. Curr Biol *19*, 1176-1181.
22. Hauf, S., Cole, R.W., LaTerra, S., Zimmer, C., Schnapp, G., Walter, R., Heckel, A., van Meel, J., Rieder, C.L., and Peters, J.M. (2003). The small molecule Hesperadin reveals a role for Aurora B in correcting kinetochore-microtubule attachment and in maintaining the spindle assembly checkpoint. J Cell Biol *161*, 281-294.
23. Vader, G., Cruijsen, C.W., van Harn, T., Vromans, M.J., Medema, R.H., and Lens, S.M. (2007). The chromosomal passenger complex controls spindle checkpoint function independent from its role in correcting microtubule kinetochore interactions. Mol Biol Cell *18*, 4553-4564.
24. Haruki, H., Nishikawa, J., and Laemmli, U.K. (2008). The anchor-away technique: rapid, conditional establishment of yeast mutant phenotypes. Mol Cell *31*, 925-932.
25. Kim, T., Moyle, M.W., Lara-Gonzalez, P., De Groot, C., Oegema, K., and Desai, A. (2015). Kinetochore-localized BUB-1/BUB-3 complex promotes anaphase onset in C. elegans. J Cell Biol *209*, 507-517.
26. Weir, J.R., Faesen, A.C., Klare, K., Petrovic, A., Basilico, F., Fischbock, J., Pentakota, S., Keller, J., Pesenti, M.E., Pan, D., et al. (2016). Insights from biochemical reconstitution into the architecture of human kinetochores. Nature *537*, 249-253.
27. Roy, B., Han, S.J.Y., Fontan, A.N., and Joglekar, A.P. (2020). The copy-number and varied strength of MELT motifs in Spc105 balance the strength and responsiveness of the Spindle Assembly Checkpoint. Elife *9*.
28. Primorac, I., Weir, J.R., Chiroli, E., Gross, F., Hoffmann, I., van Gerwen, S., Ciliberto, A., and Musacchio, A. (2013). Bub3 reads phosphorylated MELT repeats to promote spindle assembly checkpoint signaling. Elife *2*, e01030.
29. Overlack, K., Primorac, I., Vleugel, M., Krenn, V., Maffini, S., Hoffmann, I., Kops, G.J., and Musacchio, A. (2015). A molecular basis for the differential roles of Bub1 and BubR1 in the spindle assembly checkpoint. Elife *4*, e05269.
30. Zhang, G., Mendez, B.L., Sedgwick, G.G., and Nilsson, J. (2016). Two functionally distinct kinetochore pools of BubR1 ensure accurate chromosome segregation. Nat Commun *7*, 12256.
31. Tromer, E., Bade, D., Snel, B., and Kops, G.J. (2016). Phylogenomics-guided discovery of a novel conserved cassette of short linear motifs in BubR1 essential for the spindle checkpoint. Open Biol *6*.
32. Rosenberg, J.S., Cross, F.R., and Funabiki, H. (2011). KNL1/Spc105 recruits PP1 to silence the spindle assembly checkpoint. Curr Biol *21*, 942-947.
33. Garcia-Rodriguez, L.J., Kasciukovic, T., Denninger, V., and Tanaka, T.U. (2019). Aurora B-INCENP Localization at Centromeres/Inner Kinetochores Is Required for Chromosome Bi-orientation in Budding Yeast. Curr Biol *29*, 1536-1544 e1534.
34. Maure, J.F., Kitamura, E., and Tanaka, T.U. (2007). Mps1 kinase promotes sister-kinetochore bi-orientation by a tension-dependent mechanism. Curr Biol *17*, 2175-2182.
35. Biggins, S., and Murray, A.W. (2001). The budding yeast protein kinase Ipl1/Aurora allows the absence of tension to activate the spindle checkpoint. Genes Dev *15*, 3118-3129.

36. Roy, B., Verma, V., Sim, J., Fontan, A., and Joglekar, A.P. (2019). Delineating the contribution of Spc105-bound PP1 to spindle checkpoint silencing and kinetochore microtubule attachment regulation. J Cell Biol.
37. Ballister, E.R., Riegman, M., and Lampson, M.A. (2014). Recruitment of Mad1 to metaphase kinetochores is sufficient to reactivate the mitotic checkpoint. J Cell Biol *204*, 901-908.
38. Maldonado, M., and Kapoor, T.M. (2011). Constitutive Mad1 targeting to kinetochores uncouples checkpoint signalling from chromosome biorientation. Nat Cell Biol *13*, 475-482.
39. Kuijt, T.E., Omerzu, M., Saurin, A.T., and Kops, G.J. (2014). Conditional targeting of MAD1 to kinetochores is sufficient to reactivate the spindle assembly checkpoint in metaphase. Chromosoma *123*, 471-480.
40. Kruse, T., Larsen, M.S.Y., Sedgwick, G.G., Sigurdsson, J.O., Streicher, W., Olsen, J.V., and Nilsson, J. (2014). A direct role of Mad1 in the spindle assembly checkpoint beyond Mad2 kinetochore recruitment. EMBO reports *15*, 282-290.
41. Vleugel, M., Omerzu, M., Groenewold, V., Hadders, M.A., Lens, S.M., and Kops, G.J. (2015). Sequential multisite phospho-regulation of KNL1-BUB3 interfaces at mitotic kinetochores. Mol Cell *57*, 824-835.
42. Sessa, F., Mapelli, M., Ciferri, C., Tarricone, C., Areces, L.B., Schneider, T.R., Stukenberg, P.T., and Musacchio, A. (2005). Mechanism of Aurora B activation by INCENP and inhibition by hesperadin. Mol Cell *18*, 379-391.
43. Lee, S., Thebault, P., Freschi, L., Beaufils, S., Blundell, T.L., Landry, C.R., Bolanos-Garcia, V.M., and Elowe, S. (2012). Characterization of spindle checkpoint kinase Mps1 reveals domain with functional and structural similarities to tetratricopeptide repeat motifs of Bub1 and BubR1 checkpoint kinases. J Biol Chem *287*, 5988-6001.
44. Larsen, N.A., Al-Bassam, J., Wei, R.R., and Harrison, S.C. (2007). Structural analysis of Bub3 interactions in the mitotic spindle checkpoint. Proc Natl Acad Sci USA *104*, 1201-1206.
45. Mora-Santos, M.D., Hervas-Aguilar, A., Sewart, K., Lancaster, T.C., Meadows, J.C., and Millar, J.B. (2016). Bub3-Bub1 Binding to Spc7/KNL1 Toggles the Spindle Checkpoint Switch by Licensing the Interaction of Bub1 with Mad1-Mad2. Curr Biol *26*, 2642-2650.
46. Ishihara, H., Martin, B.L., Brautigan, D.L., Karaki, H., Ozaki, H., Kato, Y., Fusetani, N., Watabe, S., Hashimoto, K., Uemura, D., et al. (1989). Calyculin A and okadaic acid: inhibitors of protein phosphatase activity. Biochem. Biophys. Res. Commun. *159*, 871-877.
47. Qian, J., Garcia-Gimeno, M.A., Beullens, M., Manzione, M.G., Van der Hoeven, G., Igual, J.C., Heredia, M., Sanz, P., Gelens, L., and Bollen, M. (2017). An Attachment-Independent Biochemical Timer of the Spindle Assembly Checkpoint. Mol Cell *68*, 715-730 e715.
48. Etemad, B., Kuijt, T.E., and Kops, G.J. (2015). Kinetochore-microtubule attachment is sufficient to satisfy the human spindle assembly checkpoint. Nat Commun *6*, 8987.
49. Tauchman, E.C., Boehm, F.J., and DeLuca, J.G. (2015). Stable kinetochore-microtubule attachment is sufficient to silence the spindle assembly checkpoint in human cells. Nat Commun *6*, 10036.
50. Kuhn, J., and Dumont, S. (2019). Mammalian kinetochores count attached microtubules in a sensitive and switch-like manner. J Cell Biol *218*, 3583-3596.
51. Dick, A.E., and Gerlich, D.W. (2013). Kinetic framework of spindle assembly checkpoint signalling. Nat Cell Biol *15*, 1370-1377.
52. Kops, G., and Gassmann, R. (2020). Crowning the Kinetochore: The Fibrous Corona in Chromosome Segregation. Trends Cell Biol *30*, 653-667.
53. Aravamudhan, P., Chen, R., Roy, B., Sim, J., and Joglekar, A.P. (2016). Dual mechanisms regulate the recruitment of spindle assembly checkpoint proteins to the budding yeast kinetochore. Mol Biol Cell *27*, 3405-3417.

54. Jürg Bähler, Jian-Qiu Wu, Mark S. Longtine, Nirav G. Shah, Amos Mckenzie III, Alexander B. Steever, Achim Wach, Peter Philippsen, and Pringle, J.R. (1998). Heterologous modules for efficient and versatile PCR-based gene targeting in Schizosaccharomyces pombe. YEAST *14*, 943-951.

55. Scott, R.J., Lusk, C.P., Dilworth, D.J., Aitchison, J.D., and Wozniak, R.W. (2005). Interactions between Mad1p and the nuclear transport machinery in the yeast Saccharomyces cerevisiae. Mol Biol Cell *16*, 4362-4374.

56. Kemmler, S., Stach, M., Knapp, M., Ortiz, J., Pfannstiel, J., Ruppert, T., and Lechner, J. (2009). Mimicking Ndc80 phosphorylation triggers spindle assembly checkpoint signalling. EMBO J *28*, 1099-1110.

57. Gillett, E.S., Espelin, C.W., and Sorger, P.K. (2004). Spindle checkpoint proteins and chromosome–microtubule attachment in budding yeast. The Journal of Cell Biology *164*, 535-546.

58. Aravamudhan, P., Felzer-Kim, I., Gurunathan, K., and Joglekar, A.P. (2014). Assembling the protein architecture of the budding yeast kinetochore-microtubule attachment using FRET. Curr Biol *24*, 1437-1446.

59. Joglekar, A., Chen, R., and Lawrimore, J. (2013). A Sensitized Emission Based Calibration of FRET Efficiency for Probing the Architecture of Macromolecular Machines. Cell Mol Bioeng *6*, 369-382.

60. Khandelia, P., Yap, K., and Makeyev, E.V. (2011). Streamlined platform for short hairpin RNA interference and transgenesis in cultured mammalian cells. Proc Natl Acad Sci USA *108*, 12799-12804.